ABSTRACT

Title of dissertation:	DISCOVERY OF AN ESCHERICHIA COLI CHANNEL WITH HIGH VOLTAGE DEPENDENCE AND COOPERATIVITY.
	Shang-Hsuan Lin, Doctor of Philosophy, 2015
Directed By:	Professor Marco Colombini Department of Biology

Channels are essential for controlling the permeability of cellular membranes. The regulation of channel gating therefore plays an important role physiologically. Voltage-gating is one of the regulations that cells utilize wherein the change in transmembrane potential cause conformational changes in channels. Here a novel bacterial channel from Escherichia coli with remarkable voltage-gating properties is reported.

When the channel-forming protein was reconstituted into a planar phospholipid membrane, two different types of channel activities were observed. Type A is weakly cation-selective, with a single channel conductance about 1.5 nS (in 1M KCl solution), corresponding to a pore size of 0.9 nm. High positive voltages cause step-wise closures. Type B is voltage-independent, with much larger and noisier conductance. When LaCl3 was added, Type B channels first showed a decrease in conductance, and the residual conductance became voltage-gated, indistinguishable from Type A channels.

Under triangular voltage waves, more interesting voltage-gating behaviors were revealed. The single conducting unit seems to be composed of three channels, each with the identical 1.5 nS conductance (namely channel ①, channel ②, and channel ③). Based on the voltages at which they close/reopen, and the sequence of their closure/reopening, a model was proposed as follows. All three channels are proposed to be molecularly identical but, channel ① and channel ③ have the same orientation, which is opposite to that of channel ②. Altogether these three channels form the conducting unit in a linear array. The voltage sensor domain of each channel is proposed to take the form of a dipole moment. The interaction between dipole moments of the channels, each with an opposite orientation with its neighbor(s), leads to the impressively high cooperativity between channels. Although the physiological roles of these channels are not clear yet, the remarkably steep voltage dependence (n~14) rivals that of the channels in excitable membranes.

DISCOVERY OF AN ESCHERICHIA COLI CHANNEL WITH HIGH VOLTAGE DEPENDENCE AND COOPERATIVITY.

By

Shang-Hsuan Lin

Dissertation submitted to the Faculty of the Graduate School of the
University of Maryland, College Park, in partial fulfillment
of the requirements for the degree of
Doctor of Philosophy
2015

Advisory Committee:
    Professor Marco Colombini, Chair
    Professor David Fushman
    Professor Richard Payne
    Adjunct Professor Tatiana Rostovtseva
    Professor Sergei Sukharev

PREFACE

This dissertation shows the research I've done in the past 6 years to discover and understand the electrophysiological aspects, particularly the voltage dependence, of a novel E. coli channel. The discovery of this channel with unprecedented properties was completely unexpected. The research when I joined the lab was focused on an apoptotic protein, Bax, which forms channels on mitochondrial outer membrane to initiate the execution phase of apoptosis. The Bax protein fraction that I purified gave us remarkable voltage gating activities (following the established protocol and using the construct from Dr. Richard Youle of NIH). Same results were observed with Bax purified by Dr. Meenu Perera, a former graduate student in the Colombini lab. However, when I tried to use site-directed mutagenesis to locate the voltage sensor domain of Bax, all I obtained were negative results. Based on the 3-D structure of soluble Bax (it's usually soluble unless induced, by apoptotic signals, to form channels), 16 charged residues were picked and mutants were made for each residue (sometimes double mutations). Either single- or double-mutants were generated, by changing the residues to those with opposite charge or no charge. After failing to obtain significant different voltage-gating parameters (compared to wild-type Bax) for all of them, a question arose: is it possible that the channel former is not Bax? Since the same construct and purification protocol have been used by many laboratories, this hypothesis seemed unlikely. However, when I expressed the same plasmid with GFP in E. coli, instead of Bax (pTYB1-GFP), or even no construct, the same channel activity was observed (see Appendix). This demontrated that the channel former is not Bax. These control experiments explained why none of the Bax mutants changed the

voltage-gating behavior. Therefore, the channel former must have come from the E. coli strain that we've been using [BL21(DE3)pLysS]. With that being said, the functional data of this remarkable channel is still valid. Although Bax is the major protein in the purified samples (see Fig. 5.1 in Section 5.4.1 for the SDS-PAGE for the evidence of purity), from these control experiments, it is not involved in the voltage-dependent activities described here. Instead, a small amount of contaminant present in the widely used purification protocol used to purify Bax contains the active channel former. Chapters 3 and 4 contain the 2 papers published at a time when we were convinced that Bax was responsible for the channel-forming activity. The results are valid but the interpretation reflects our understanding at the time.

The first chapter presents an introduction to channels in general and the regulation of their gating. Later in the chapter, E. coli and channels in this bacterium are introduced. Finally, examples of other voltage-gated channels are covered, particularly their electrophysiological properties and gating mechanisms.

The materials used in the experiments are listed in Chapter 2. Detailed protocols and their rationale are also described in this chapter, from how the samples were prepared, how each experiment was set up and under what conditions, to how the data were analyzed and interpreted.

The experimental results start with Chapter 3. In this chapter, the basic electrophysiological properties are shown, including the conductance, selectivity, voltage dependence, etc. Moreover, I found that the channel showed two distinct types of activities, namely Type A and Type B. The conversion between them can be done with the addition of $LaCl_3$. Experiments were done with the planar phospholipid

membrane system. This work was published in Biophysical Journal in 2011, and also laid the foundation for the following chapter. Fellow graduate student Meenu Perera provided me with guidance and invaluable suggestions; undergraduate students Toan Nguyen, Debra Datskovskiy, Megan Miles, Brian Bujarski, Sajeela Padder, and Stephanie Fischer assisted with the experiments on planar membranes.

In Chapter 4, a more detailed manipulation of the input voltage signals allowed us to probe the voltage-gating behaviors. Furthermore, these behaviors helped us to build a molecular model of how the channel-forming entities interact with each other through the dipole-dipole interaction and contribute to the remarkable gating observed. Additionally, the voltage-gating parameters, the kinetics and the cooperativity between channels are also discussed here. This work was published in Biochemical Journal in 2013. Undergraduate students Nuval Cherian, Benjamin Wu, Hyo Phee and Christy Cho assisted with the experiments on planar membrane and data analysis.

In the final chapter, a discussion of the behavior/model, ongoing work and future directions are presented. I am working with fellow graduate student Kai-Ti Chang in attempts to identify the channel-forming protein.

DEDICATION

I would like to dedicate this dissertation to my parents, Kuang-Hsin Lin and Ing-Tai Ho, and my husband Brian Bujarski.

ACKNOWLEDGEMENTS

students I've ever seen. I really miss the time that we worked in the lab together, trying to understand this channel. Nuval Cherian, Benjamin Wu, Hyo Phee, Christy Cho, Jordan Cohen, Jenny Kunselman, Rachel Peissner, Bernadette Butcher, Matthew Kovacs, Gohar Avagyan, Steve Devlin, Jason Hauzel, and Stephanie Fischer: thank you all for contributing to the work. It is a wonderful experience to teach you and figure out the important scientific questions together.

To my family, my in-laws, and friends here and abroad, thank you all for being available and supportive when I needed you. Being here in the U.S. for graduate school is not the easiest thing to do. I'm really grateful to have you who love me and care about me, and that give me the strength to pursue my career in science.

TABLE OF CONTENTS

LIST OF TABLES

LIST OF FIGURES

CHAPTER 1: **GENERAL INTRODUCTION**

1.1 Channels

1.1.1 Classes of Channels

Channels are passive pathways for ions/molecules/metabolites (must go down their electrochemical potentials) to translocate between different compartments within the cells or between the cells and the environment. These transmembrane entities contribute to the permeability of the membranes in which they reside: determining the type of permeating molecules and the amount of flux. Membrane channels have been found to be involved in many diseases (channelopathies), including osteoporosis [1], cystic fibrosis [2], and many nervous/muscular system disorders [3,4], etc. Here several types of channels are introduced that differ in structure and origin. Note that although more than 400 genes are known to encode for channels, many aspects of the structure and function of channels remain unclear.

1.1.1.1 Proteins

This is probably the most common and well-studied class of channels. In general, proteins may interact with the membranes in several ways: direct or indirect binding to lipids, loosely attached or transmembrane, single-pass or multi-pass (number of transmembrane domains). In order to form a channel, the proteins must be transmembrane and thus possess a great deal of secondary structure. Channel-forming proteins tend to be either mainly α-helical or β-barrel. β-barrel channels are common in the outer membrane of mitochondria, chloroplasts, and bacteria. Most mammalian channels are predominantly α-helical. A classical example of highly α-helical channel-formers is the family of sodium/potassium/calcium channels. The voltage-dependent

2

anion-selective channels (VDAC) in mitochondria are essentially β-barrels. In addition to the secondary structures, the pore sizes and selectivity of the proteinaceous channels can be quite different as well. Some porins and gap junctions are relatively nonselective and large whereas the ion channels and aquaporins are highly selective in, that only certain molecules/ions are allowed to pass.

1.1.1.2 Toxins

Toxins are the substances produced by a wide variety of organisms, ranging from microorganisms, plants to animals, for the purpose of either predation or defense. Due to the space limitation, this section only focuses on bacterial toxins. Upon infecting the host, bacterial toxins usually result in physiological malfunction, or even death. They may attack the target cells in a variety of ways, such as inhibition of protein synthesis, disruption of transmembrane signal transduction, or disorganization of cytoskeleton, etc [5]. More importantly, about 30% of them are membrane damaging/pore-forming, making them the largest group of virulence factors [6].

The pore-forming toxins (PFT), unlike others, do not have enzymatic activities. Instead, these toxins form channels in the cytoplasmic membrane of host cells either to kill the host cells (e.g. immune cells), or to retrieve nutrients (e.g. red blood cells). PFTs can be categorized by their structures (α-helical or β-barrel), sequences (e.g. the family of RTX toxins all share a common nonapeptide sequence repeats) [7], or functions (e.g. the family of CDC toxins are the cholesterol-dependent cytolysins).

RTX toxins form cation-selective channels of varying diameters. α-hemolysin (HlyA) is the prototype of this group of toxins. RTX toxins seem to prefer forming channels in membranes containing a mixture of lipids (e.g. asolectin) rather than

membranes formed from a pure lipid. The conductance of these channels varies about 100-fold [8]. The electrophysiological properties are also rather variable. For example, the single channel conductance of ApxIII is about five times smaller than that of ApxI (from A. pleuropneumoniae) [9]. Note that most of the RTX toxins only have limited open-channel lifetime. The mean lifetime for the HlyA channels of E. coli is about 2 seconds [10], and that for the HlyA of M. morganii and P. vulgaris are 27 and 32 seconds, respectively [11]. Other classical examples of pore-forming toxins include colicins, anthrax toxin, and gramicidin. A comparison of the properties of several PFTs is shown in Table 1.1.

Table 1.1 Properties of some toxin and peptide channels

Organism	Protein/peptide	Open channel conductance (pS)	Selectivity (Pc/Pa)	Pore size (nm)	# of monomers	Structure	Voltage-dependence
E. coli [10]	HlyA	520 δ	14 θ	2.6	8	β-strand	Open at negative, close at positive [12]
A. pleuropneumoniae [9]	ApxIII	95 δ	9.6 Ω	1.8	-	-	-
B. pertussis [13]	CyaA	4.8 μ	10 θ	<0.62 [14]	>1 [15]	α-helical	-
E. coli	Colicin E1	24 ε [16]	0.14 χ [16]	0.8 [16]	1	α-helical	open at >=30 mV, close at <= -30mV [17]
B. brevis	Gramicidin A	8 ψ [18]	Ideal selectivity for monovalent cation [19]	0.4 [18]	2	β-helical	Higher positive voltages promote channel formation [12]
A. mellifera (honey bee venom)	Melittin	110 φ [20]	<1 [20]	1~6 [21]	4 [22]	α-helical	Higher positive voltages promote channel formation [22]
H. sapien [23]	Aβ25-35	10~400 ρ	1.6 τ	various	>1 [24]	β-strand	Open at positive potentials and close at negative potentials

δ: 150 mM KCl
μ: 100 mM KCl
ε: 1.0 M KCl
ψ: 500 mM NaCl
φ: 1.8 M NaCl
ρ: 100 mM NaCl

θ: 50: 500 mM KCl gradient
Ω: 10: 100 mM KCl gradient
χ: 100: 1000 mM KCl gradient
τ: 100: 1000 mM NaCl gradient

5

1.1.1.3 Small Molecule Channels: Peptides and Lipids

Peptides

Short polypeptides are also able to permeabilize membranes and form channels. Some animal and plant cells secrete channel-forming peptides and these serve an antimicrobial function. They serve as a fast-reacting defense. Although the sequences, the structures, and the functions vary greatly, they generally share the following features. First, the length of the peptide is usually about 12-50 amino acids, with no significant homology. Typically these peptides are cationic (+2~ +9) [8]. Secondly, these antimicrobial peptides are amphipathic. With these features the antimicrobial peptides do not need the help of a receptor to bind to the membrane (which is not the case for many toxins) and form channels.

Some channel-forming peptides are produced during chronic, progressive diseases. For example, the amyloid peptides produced during Alzheimer's disease have been reported to form channels. These may be related to the pathologic mechanism of the disease. The amyloidogenic peptides are usually small (3-30 kDa), anionic, and identified by their characteristic staining by Congo red. These peptides homomerically aggregate and form fibrils in certain tissues. The amyloid peptide channels typically have a variety of conductances, weak selectivity, and a long lifetime [8]. See Table 1.1 for the biophysical parameters of some peptide channels.

Lipids

Ceramide channels are the only described long-lived lipidic channels. The physiological level of ceramide molecules increases during apoptosis [25–27]. Besides serving as a secondary messenger for multiple cellular processes, ceramide molecules

were also found to form stable, large channels. The intermolecular hydrogen-bonding of the ceramide molecules has been proposed to form "columns" and these arrange themselves in an anti-parallel fashion to form barrel-stave channels [28]. The main function of ceramide channels is to induce apoptosis through permeabilizing the mitochondrial outer membrane [29]. These ceramide channels are found to have a typical diameter of about 10 nm [28,30]. It has also been found that ceramide channels are regulated by Bcl-2 family proteins, which regulate apoptosis [31,32].

1.1.2 Regulation of Channels

Channels are regulated in a variety of ways. Channel gating is often controlled by chemical, thermal, mechanical, or electrical energy. Gating results in a change in permeability and other biophysical properties. Sometimes a channel gating is controlled by more than one method.

1.1.2.1 Ligand-gated

Ligand-gated channels are channels that regulate the ion flux through the binding of specific ligands. Ligand-gated channels are involved in medical conditions such as ischemic stroke, nicotine addiction. The transmission of signal across the synaptic cleft is achieved by the binding of neurotransmitter (secreted from the presynaptic neuron) to the ligand-gated channels of the postsynaptic cell. The ligand-gated channels then open, allowing ions such as Na^+, K^+, Ca^{2+}, Cl^- to flow through. This process allows the chemical signal being converted into electrical signal, either depolarizing or polarizing the local membrane. Compared to the voltage-gated channels, the ligand-gated ones are less sensitive to the transmembrane potential. Additionally, the binding and thus the gating process is only transient: the

neurotransmitters are usually removed by enzymes or the neurotransmitter transporters. Therefore, they themselves cannot account for the generation and propagation of action potential, which is achieved by the voltage-gated ion channels. In order to complete these important tasks, the ligand-gated channels are usually very specific, in both the binding sites for neurotransmitters (i.e. only responsive to certain ligands) and the selectivity filter of the channel lumen (i.e. only allows specific ions to flow). Examples of the ligand-gated channels include the acetylcholine receptor, ATP-gated channels, and glutamate receptors, etc.

1.1.2.2 Voltage-gated

Voltage-gated channels, as the name suggests, are channels whose gating process (open or closed) is controlled by the transmembrane potential. To do so, there must be a voltage sensor domain (VSD) within the channel. The voltage sensors of voltage-gated channels are usually charged and move through the field when the membrane potential is changed, resulting in conformational changes; i.e. as the channel opens or closes. Voltage-gated channels are important in controlling the membrane potential of animal cells and the generation of an action potential. Moreover, functions such as the synchronization of cells through electrical synapses (connexins), the flow of molecules across the mitochondrial outer membrane (VDAC), etc. are also controlled by voltage-gated channels. However, still some channels that are voltage-gated *in vitro* may have little impact *in vivo* (or the physiological importance has yet to be found). Standard parameters such as V_0 (the voltage that causes half of the channels close) and n (the number of charges that would need to move through the entire field to account for the steepness of the voltage dependence) are commonly used to

quantitate the voltage gating. These parameters can be obtained by using the Boltzmann distribution. See more detailed information about the gating mechanisms, examples, and their physiological importance in Section 1.3.

1.1.2.3 Mechanosensitive

Mechanosensitive channels change their structures/diameters with the mechanical stress that they receive, which can come from a variety of sources: touch, sound wave, osmotic pressure, etc. Two main mechanisms are proposed: (1) The mechanical tension comes from the lipid bilayer, and then the channels are open/closed accordingly. (2) The channel are actually being "pulled" open by the displacement of the cytoskeleton and/or the extracellular matrix, through a tether [33]. Through these mechanisms, the mechanosensitive channels are able to convert the mechanical stimuli into electrical or biochemical signals for downstream regulations. In bacteria, the mechanosensitive channels are essential for their osmosensing. For example, the MscL channel has a conductance of 2.5 nS (200 mM KCl, 40 mM $MgCl_2$) [34], which is quite large compared to eukaryotic channels. This feature allows MscL to be the "emergency valve" when the bacteria experience a sudden osmotic shock. MscL is non-selective [34], while the smaller MscS is anion-selective (P_K:P_{Cl}=0.33~0.67) [34]. Besides these bacterial channels, examples such as TREK-1 in mammals, Piezo in mammals and plants, are also mechanosensitive channels that regulate many functions (e.g. pain perception, vasodilatation).

9

1.2 E. coli Channels

1.2.1 General Introduction to E.coli

E. coli is a Gram-negative, rod-shaped bacterium, which is commonly used in the laboratories for its ease to culture, sequenced genome [35], and many engineered common strains for different purposes. Due to the fact that the genomes of many strains are already known [36], one can easily transform constructs into E. coli and manipulate the production of desired proteins/plamids [37,38].

Physiologically, E. coli is commonly found in the intestines of warm-blooded animals. Being one of the most diverse bacterial species, E. coli strains only share 20% of genes in common [39] (only a small fraction of E. coli is pathogenic). Therefore, while some of the strains are used as probiotics for therapy [40,41], others can cause diseases like urinary tract infection [42], neonatal meningitis, pneumonia [43], etc.

To understand the channels in E. coli, one must first consider the environments in which these channels sit. Just like other Gram-negative bacteria, the cell envelope of E. coli consists of three parts [44]: the outer membrane (OM) [45,46], the periplasmic space, and the inner membrane (IM). More than just simple boundaries, these three layers and proteins from them covalently or noncovalently interact, to contribute to the structure of the cell and then facilitate other functions (e.g. biogenesis of membrane proteins). For example, the cell shape is generally determined by the peptidoglycan layer in the periplasmic space due to its rigidity. Spheroplasts are cells that lose their characteristic shapes after the peptidoglycan layers being removed. Outer membrane proteins such as the lipoproteins (covalently) [47] and OmpA (noncovalently) [48] bind to the peptidoglycan layer and contribute to the structural stability of the cell envelope. The

biogenesis of the outer membrane and OM proteins also shows how the protein complexes in these three layers work together. A good example would be the biogenesis of many porins: the outer membrane protein precursors first synthesized in the cytoplasm, then transported by SecYEG in the IM, modified by chaperon SurA in the periplasmic space, then finally assembled by the Bam machinery in the OM.

1.2.2 Outer Membrane

The outer membrane (OM) is a special feature of Gram-negative bacteria and different from most other membranes found in living organisms. While the inner leaflet of the outer membrane is composed of phospholipids, the outer leaflet is primarily composed of the lipopolysaccharide (LPS) [49]. A LPS molecule has three parts: lipid A, oligosaccharide core, and polysaccharide (O-antigen). Due to the six saturated fatty acid chains of lipid A (compared to two in phospholipids), the LPS is much more hydrophobic than the regular phospholipid. The polyanionic LPS molecules are cross-linked by divalent ions and thus form a strong permeability barrier to the entry of small hydrophobic molecules, such as antibiotics, detergents, etc. [50] This allows Gram-negative bacteria to be less susceptible to difficult environments, compared to Gram-positive bacteria. The Braun's lipoprotein (BLP), with its abundancy ($>10^5$ per cell) and covalent attachment to the peptidoglycan layer, is another important molecule that contributes to the structure and integrity of the OM [51]. Additionally, the permeability of the OM is mainly determined by porins. These transmembrane proteins form pores to allow the selective exchange of molecules between the periplasmic space and the environment.

Porins are generally composed of trimers of β-barrels. These proteins can be grouped into several categories, considering their structures and functions. The largest group is the general diffusion porins (e.g. OmpF, PhoE), followed by the specific porins (e.g. LamB for maltodextrin). Transport porins are another category. The diameter of their pores are larger than those of the general diffusion porins due to the presence of an internal stopper domain (e.g. FhuA, BtuB) [52,53]. This category of porins is energy-dependent: they utilize the energy transduced from the inner membrane protein complex to function. Additionally, some porins have quite limited conductance/pore size. Instead of being a pathway for molecules to enter the cell, they are thought to act as anchors for others to bind to the surface (e.g. OmpA) [54], such as small-molecule nutrients , bacteriophages, etc [55]. In the case of the general diffusion porins, extracellular loop L3 and the adjacent barrel wall together form the constriction zone that determines the permeation limit for the porins. From the molecular dynamics data, this structural feature may also facilitate the translocation of molecules (e.g. penicillin) through electrostatic interaction with the constriction zone [56,57]. Mutagenesis studies also confirm the importance of this constriction zone [58–60]. pH and polyamines are found to change the properties of the channels in the porins. For example, acidic pH increases the probability of the closed state in OmpF [61], whereas polyamines appear to bind to the channel lumen and induce closures [62–64]. A list of the biophysical properties of some porins are listed in Table 1.2. Overall, porins from different categories show quite different properties (e.g. OmpC, OmpF, PhoE are from the general diffusion porin

category, whereas FhuA is the transport protein). Even within the same category the biophysical properties vary (e.g. OmpC is cation-selective, but PhoE is anion-selective).

Table 1.2 Properties of some porins

	Open channel conductance (nS) [μ]	*Selectivity (Pc/Pa)* [Ω]	*Pore size (nm)*	*# of monomer*
OmpC	1.5 [65]	26 [65]	1.0 [65]	3
OmpF	2.1 [65]	3.6 [65]	0.7 [66] or 1.2 [65]	3
PhoE	1.8 [65]	0.3 [65]	1.1 [65]	3
LamB	2.7/0.2 [65]	4.5 [65]	1.4 [65]	3
FhuA	-	-	3.9 x 4.6 [67 δ]	1
OmpA	0.6 [68 θ]	0.66 [68 λ]	0.6-0.7 [68]	1

μ: 1 M KCl, unless otherwise listed
θ: 1M NaCl
Ω: 0.01 M/ 0.1 M KCl gradient, unless otherwise listed
λ: 0.1M/0.7M KCl gradient
δ: Elliptical cross-sectional area

1.2.3 Periplasmic Space

The periplasmic space sits in between the outer and inner membranes. A layer of peptidoglycan in the periplasmic space provides structural support to the cell (due to its rigidity), acts as a binding site for inner and outer membrane proteins, and the home for some binding proteins, degradative or detoxifying enzymes, sensing proteins, etc. The peptidoglycan is composed of alternating disaccharides N-acetyl-glucosamine (NAG) and N-acetyl-muramic acid (NAM). Each NAM is attached to an oligopeptide chain, and then each oligopeptide chain is linked with the neighboring oligopeptide chains through an amide linkage (in the case of E. coli) [69,70]. Due to the cross-linked

network, the peptidoglycan is a fairly strong and rigid structure. Antibiotics such as penicillin kill the bacteria through disturbing the synthesis of the peptidoglycan.

1.2.4 Inner Membrane

The inner membrane (IM), unlike the outer counterpart, is mainly composed of phospholipids: about 80% phosphatidylethanolamine, 15% phospatidylglycerol, and 5% cardiolipin. Not surprisingly, the membrane proteins found in these two membranes are quite different. ATP transporters, ABC exporters, RND (resistance-nodulation-division) efflux pumps, are some examples of inner membrane transport proteins. One mainly finds transporters in the inner membrane, since the existence of channels may dissipate the transmembrane potential across the inner membrane. Moreover, most of the integral membrane proteins found in the IM are α-helical. Unexpected electrical spikes resembling the action potential signal in neurons were detected in E. coli using fluorescent voltage-indicating proteins [71]. It may be an indication of the existence of voltage-gated channels in the inner membrane. Generally, due to the small size and the cell wall, it is more difficult to study the bacterial electrophysiology, compared to the eukaryotic cells.

1.3   *Voltage-gated Channels*

Voltage-gated channels are defined as channels that have conformational changes (open or closed) coupled to the membrane potential. These channels are found in many organisms, both eukaryotes and prokaryotes. Many of these channels are highly conserved among organisms. Here are some classical examples.

1.3.1 Potassium/Sodium/Calcium Channels

This is probably the most intensively studied group of voltage-gated channels. They are typically found in the plasma membranes of animal cells. Ever since the famous quantitative analysis of the action potential by Hodgkin and Huxley [72], the research on these channels that are responsible for the electrical excitability of cells, has increased dramatically. The structures of the proteins in this group share many common features. From the X-ray crystal structures of several K_v channels, voltage-gated potassium channels are homotetrameric [73–75]. Each monomer is composed of 6 transmembrane segments (S1 to S6) [76,77]. Among these helices, S4 is the voltage sensor domain (VSD). By having 4-8 positive charges, S4 helix can sense the change in voltage and move accordingly [78]. The channels open when S4 charges face the extracellular side. This sensor domain is highly conserved among all voltage-gated potassium, sodium and calcium channels. For voltage-gated sodium and calcium channels, each monomer/channel consists of four non-identical repeats of the S1-S6 transmembrane domains. For each family (K^+, Na^+, or Ca^{2+}), there are a large number of different isoforms [79]. Nevertheless, they all share a similar gating mechanism.

Generally, when the membrane potential changes to the appropriate level, the S4 helix starts to move. This movement propagates to the S5, S6 helices, resulting in channel closure. Besides the closed and open states, there is also an inactivated state for many of these channels. After the open state, channels get into this closed conformation that can't be activated (even with the right membrane potential). Inactivation used a ball-and-chain mechanism. The N-terminus of the channel forms a "ball", linked to the rest of the channel through a short polypeptide "chain"[80]. The ball

domain blocks the channel inducing the inactivation state. While S4 accounts for the voltage sensor, a highly conserved sequence forms the pore and determines the selectivity of the channel ("TVGYG", in the case of potassium channels) [78].

Being selective is quite important for channels in this group. Probably the most well-known function of these channels is their role in the excitability of cells. Voltage-gated potassium channels and sodium channels together are responsible for the action potential, critical to the function of muscle cells and neurons. Besides these well-known functions, voltage-gated calcium channels are responsible for activating certain potassium channels, and the regulation of hormone release, etc. In order to accomplish these tasks, the voltage-gated ion channels have to be both highly selective (e.g. differentiate K^+ and Na^+) and generate a high rate of ion flux (millions of ions flow in a millisecond) [78,81]. These characteristics of voltage-gated ion channels are achieved through the selectivity filter which interacts intimately with the permeating ions [82]. The single file of permeation through multiple binding sites results in electrostatic repulsion, destabilizing the bindings sites, and achieving high flow rates [83–85].

Due to the physiological importance of these channels, malfunction of these can cause serious problems. Certain toxins attack cells by targeting at these channels. For example, tetrodotoxin (secreted from fishes in the order of Tetraodontiformes) inhibits the formation and propagation of action potential by blocking the voltage-gated sodium channels [86]. Diseases like ataxia, epilepsy, are tightly linked to the mutations in these channels [87,88].

16

1.3.2 Large Eukaryotic Voltage-Gated Channels: VDAC and Connexin

1.3.2.1 Voltage Dependent Anion-Selective Channel (VDAC)

VDAC stands for Voltage Dependent Anion-selective Channel. It's one of the most abundant proteins on the mitochondrial outer membrane (MOM). This channel is highly conserved among all eukaryotic kingdoms, from mammals, plants, fungi to protists [89–92]. Unlike the voltage-gated potassium/sodium/calcium channels, VDAC, as the name suggests, is selective for anions, more specifically, for metabolic anions. This monomeric, β-barrel channel is the main pathway by which anionic metabolites translocate between the cytosol and the mitochondrial intermembrane space.

There are three major conformational states of VDAC: one open state and two closed states. When the membrane potential is close to zero, the channel is in the open state. Both positive and negative membrane potentials (> 30 mV) induce the closure of VDAC to a variety of lower conductance closed states [93,94,95]. There are three isoforms of VDAC in humans: VDAC1, VDAC2, VDAC3, with VDAC1 being most abundant and well-studied. From the selectivity, pore size (2.5 nm at the open state, 1.8 at the closed state) [96–98], and other functional experiments [96,99–101], the gating process was deduced. Upon channel closure, the positively charged voltage-sensor domain moves outside of the pore (to either the cytosolic side or the intermembrane space side), leaving a pore with smaller diameter, opposite selectivity (cation-selective), and less volume. It also becomes impermeable to ATP.

From the functional data, 13 β strands and 1 α helix have been shown to form the pore of the channel [100]. From mutagenesis data, specific regions have been shown to be the voltage sensor. Structural approaches, NMR and X-ray crystallography, were

used to solve the 3-dimensional structure of VDAC1 that was refolded from the denatured state in inclusion bodies [102–104]. The solved structure is a 19 β-stranded barrel with the 1 α helix in the pore. However, due to many inconsistencies with the functional data, this structure may not be the native/functional one [105].

Nevertheless, VDAC has been found to have great physiological importance. One of the metabolites that passes through VDAC is ATP. Many ATP-dependent metabolic pathways have been found to be related to VDAC. It's been reported that VDAC interacts with the cytoskeleton [106,107]. VDAC has also been implicated in regulating Ca^{2+} homeostasis [108]. Because of the key role that mitochondria plays in cell life and death, the possible involvement of VDAC in apoptosis has been studied as well [109,110]. Links between VDAC and diseases like Down syndrome [111], Alzheimer's disease [111], cancers [112] and influenza [113] have been hypothesized as well.

1.3.2.2 Connexin

Connexins are also called gap junction proteins. Six connexin monomers form a connexon (hemichannel), and the hemichannels from each of the membranes to be connected combine to form the gap junction. Although the connexin family is quite diverse (21 members) [114], the connexin protein generally has four transmembrane domains with loops on both the extracellular and the cytosolic sides. Through head-to-head docking, homomeric (formed by identical connexins) or heteromeric (formed by different connexins) hemichannels can constitute the gap junction. What makes connexins special is that they form intercellular voltage-gated channels as well as single channels on the plasma membrane (named undocked hemichannels).

The diameter of the pore is about 1.5 nm. In general, the properties of intercellular connexin channels vary widely, depending on the composition of the channels. The selectivity, for instance, ranges from anion-selective to cation-selective. The single channel conductance could be in between 5 to 300 pS [115,116]. Most connexins are only sensitive to the transjunctional voltage (V_j, the difference of the membrane potentials of two cytoplasms that are connected through the gap junction) [117]. Basically there are two proposals for the gating mechanisms. First is that the N-terminus is the voltage sensor, based on studies of Cx26 and Cx32 [118–120]. The second mechanism indicates that the C-terminus may bind to the cytoplasmic loop and close the channels, from experiments on Cx43 and Cx40 [121–123]. Apparently, the composition of the subunits matter when one tries to investigate the properties of the channel.

Both intercellular channels (gap junctions) and undocked hemichannels are involved in several physiological events. The intercellular channels can form the electrical synapses in the excitable membranes of the heart and the brain, and they can also help to synchronize cellular activities in non-excitable tissues. For the undocked hemichannels, their open probability is found to be regulated by the extracellular concentration of calcium, and hence manage the threshold for action potential. For example, lower extracellular $[Ca^{2+}]$ increases the open probability of the undocked hemichannels, leading toward membrane depolarization [124,125]. At least fifteen diseases are linked to the genetic mutations of the connexins [126]. Among them, change in function of voltage-gating is one of the causes [127].

1.3.3 Prokaryotic Channels: Porins

Porins are a family of proteins found in the outer membrane of gram-negative bacteria. They allow hydrophilic molecules to travel between the environment and the periplasmic space. Besides Wza [128], typically all the porins are β-stranded barrels. Common porins include PhoE, OmpC, OmpF (from enterobacteria) and PorB (from Neisseria), etc. Like many others, these porins are composed of 16 β strands, and form trimeric channels.

Although some of them were found to be voltage-gated [129], the steepness of the voltage dependence is low and the physiological importance of the voltage dependence is unclear. Mainly it's due to the fact that the voltage required for gating seems to be out of the physiological range: 130 mV for OmpF [130], for instance. Some porins gate at more physiological voltages (e.g. PorB closes around 40-50 mV) [131]. When tested, the conductance of OmpF and OmpC do not seem to be affected by generated Donnan potentials (5 mV to 100 mV). Therefore, the voltage-dependency of general porins are proposed to be just artificial effects in *in vitro* experiments [132]. However, it has been proposed that the voltage-gating properties can actively close porins that accidentally insert in the inner membrane [133] and thus perhaps this is their function. The voltage gating is sensitive to environmental conditions. Several parameters have been reported to affect the voltage-gating behaviors, including the pH [130,134], lipopolysaccharide [135,136], polyamine [64,137,138], or even how the bilayers were formed [139]. Overall, the physiological relevance of voltage gating remains unclear.

Experiment to identify the voltage gating domain of some porins were not successful. The L3 loop of porins, due to its localization at the constriction zone, was

proposed to be involved in the voltage gating [140]. However, from simulations [141] and from mutagenesis experimental results [142,143], it is generally accepted that L3 loop does not move by much during the gating process. In addition deleting this loop does not affect the voltage dependence. Besides L3, the extracellular loops were investigated for their role in voltage gating. Structural work [144], mutagenesis [145] and chemical modifications [146] were done to elucidate this hypothesis. The efforts were unsuccessful.

Regardless of the molecular mechanism for voltage dependence, the fact remains that the porin channels in E. coli reported to date show a rather weak voltage dependence that may arise from the electrical polarity of the structure and thus may be a side effect of a structure that has a different function. The high electric field required for voltage gating distorts matter and can result in electrical breakdown that is unrelated to the function of the material. However, the channel former described in the following chapters displays a very steep voltage dependence, rivaling that of the channels in animal cells responsible for electrical excitability. Thus, these must have an important physiological function awaiting to be discovered.

Table 1.3 Properties of some voltage-gated channels

	Open channel conductance (1M KCl)	Selectivity (P_c/P_a, 0.1M/1M KCl)	Pore size (nm)	n value (gating charge)	V_0 (mV)	# of monomers
K$^+$ channels	3.7 pS ρ [147]	-	0.4 [148]	4(14) [149–151]	-58 (fast) or 7 (slow) [152]	4
VDAC	4.5 nS [153]	0.59 [154]	2.5 [107]	2 [155], 4.9±0.5 or 3.6±0.2 [156] φ	-28 ± 4, 5.2 ± 0.4 [156]	1
OmpF	0.84 ± 0.06 nS [157]	3.5 ± 0.5 [158]	0.7 [66]	-	145 ± 7 [157]	3

ρ: 140 mM KCl
φ: Depending on the experimental conditions.

22

CHAPTER 2: **MATERIALS AND METHODS**

Diphytanoylphosphatidylcholine and asolectin were purchased from Avanti Polar Lipids. Cholesterol was obtained from Sigma. BCA protein assay kit, the 12% Tris-HEPES protein gels, and the silver stain kit were purchased from Thermo Scientific. All other chemicals were reagent grade.

2.2 Methods

2.2.1 Electrophysiological Recordings

2.2.1.1 Planar Phospholipid Membrane

Planar phospholipid membranes were formed by the monolayer method [159,160]. Each side of the Teflon chamber contains 5 mL of the desired salt solution, separated by a 0.1-mm hole in the polyvinylidene chloride (PVDC) partition (Fig. 2.1). 5% petrolatum (w/v) in petroleum ether was used to smoothen the edge of the hole and to help the formation of bilayer membrane. This coating was left for 15 minutes for the solvent (petroleum ether) to dry before the aqueous solution was introduced into the chamber. The monolayers were formed by layering 30-60 µL of the lipid solution [0.5% DPhPC (diphytanoyl phosphatidylcholine), 0.5% asolectin (polar extract of soybean phospholipids) and 0.05% cholesterol in hexane] on the surface of the aqueous solutions [0.1-1.0 M KCl (depending on the experimental design), 1 mM MgCl2 and 5 mM Pipes (pH 6.9)] on either side of the partition. The solvent of the lipids was allowed to dry for 5 minutes. One then can control the level of the solution with the syringes connecting to each side of the chamber. Calomel electrodes were used to interface with the aqueous phase. The membrane voltage was clamped using a high-

quality operational amplifier in the inverted mode and the current recorded using Clampex 10.3 software. One first raised the level of the aqueous solution of the *trans* side (maintained at virtual ground by the amplifier) to just above the hole forming a monolayer across the hole. Afterwards, the level of the aqueous solution of the *cis* side was raised to match the *trans* side. When the monolayers from both sides meet across the hole, the phospholipid bilayer membrane is formed. The formation of the phospholipid bilayer membrane was monitored using an oscilloscope. A square voltage wave was applied to the membrane and the capacitive transients monitored, as well as any change in current. The increase in capacitance indicated the formation of
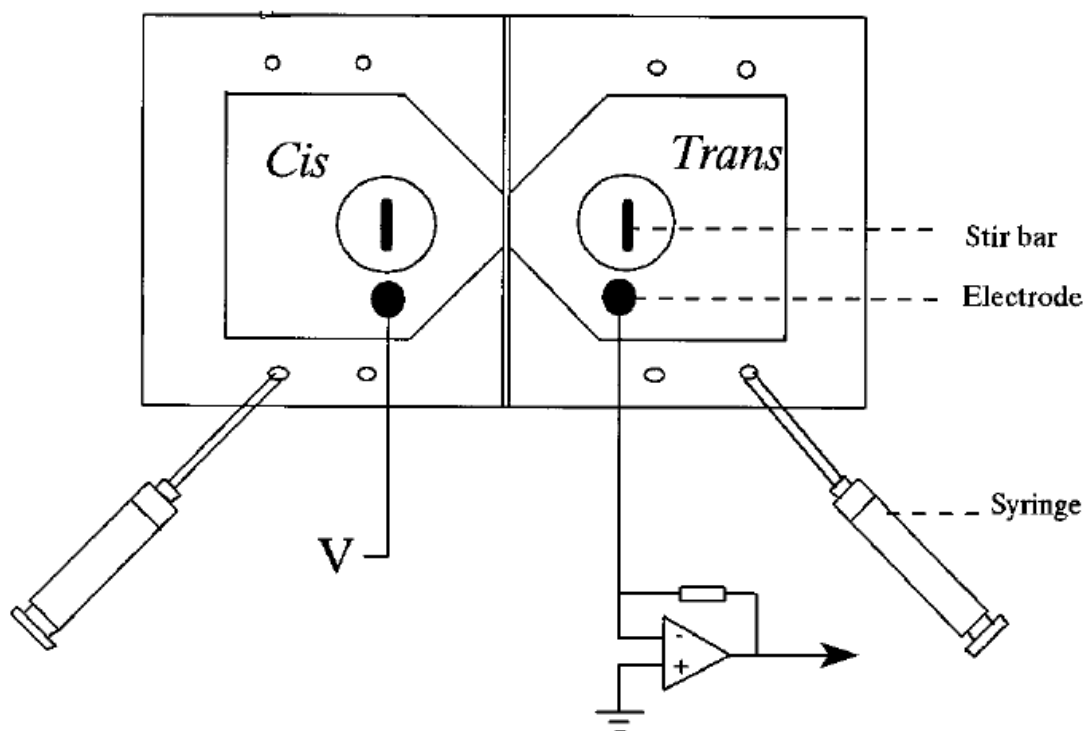
Fig. 2.1   Experimental setup for planar phospholipid membrane experiments.   Two compartments (*cis* and *trans*) are separated by a PVDC partition. The *trans* side is maintained at virtual ground by the amplifier. This research was originally published in The Journal of Biological Chemistry. Xu, X, Colombini, M. Self-catalyzed insertion of proteins into phospholipid membranes. *J. Biol. Chem.* 1996; 271: 23675-82. © the American Society for Biochemistry and Molecular Biology.

the membrane.   No detectable current increase indicated a membrane with low

conductance. Only membranes with low conductance ($<$ 0.05 nS), stable under high voltages and stirring, were used for experiments.

Typically 20–50 μl of the sample was dispersed in 5 ml of aqueous solution on one side of the membrane while stirring. The sample was pretreated with β-octyl glucoside to 1% (w/v) for at least 15 min on ice. No channel-forming activity was detected without this treatment and addition of only the β-octyl glucoside did not produce any channels. Voltage ramps were applied to investigate the behavior of these channels and determine their voltage-gating parameters. All the results reported were observed in at least three independent experiments, with usually multiple repeats of the illustrated behavior within each experiment.

2.2.1.2 Data Acquisition, Correction and Calculation

The amplifier was wired in the inverted mode with an adjustable feedback resistor (R_f). Typically 10^8 Ω resistance was selected. Data were generally low-pass filtered at 500 Hz, but in some experiments this was reduced to 5 kHz. Before the addition of the sample, any offset in the recording was either adjusted or recorded. After the experiments were completed, the electrode asymmetry was measured and recorded. For asymmetric aqueous solutions (e.g. 1.0 M KCl on the *cis* side and 0.5 M KCl on the *trans* side), the liquid junction potential was calculated and used to correct the measured electrode asymmetry. For this calculation, the Nernst/Plank steady state equation (Equation 1) was used, where u represents the ionic mobility. The conductance at any point in the experiment was calculated using Equation 2.

The selectivity (permeability ratio of cations over anions) of a channel in the presence of a salt gradient was calculated by using the Goldman-Hodgkin-Katz

26

Equation (Equation 3) [161,162]. P, here, represents the permeability. From the conductance of a single channel an estimation of the diameter of the channel opening was obtained assuming that the conducting pathway is an uncharged right cylinder, 5nm in length (Equation 4)[163]. The estimation corrected for the access resistance. d is diameter (cm); G here is conductance (S); λ is conductivity (cm^{-1} S); and L is the length of channel (cm).

$$\Delta\varphi_{liq} = \left(\frac{u_{K^+} - u_{Cl^-}}{u_{K^+} + u_{Cl^-}}\right) \times \frac{RT}{F} \times \ln\frac{[KCl]_{trans}}{[KCl]_{cis}}$$ ....Equation 1

$$Conductance = \frac{current}{voltage} = \frac{\frac{-(V_{current} - offset_{current})}{R_f} \times \frac{1}{gain_I}}{\left(\frac{V_{voltage} - offset_{voltage}}{gain_v}\right) - \Delta\varphi_{rev} - (electrode\ asy. - \Delta\varphi_{liq})}$$

....Equation 2

$$\Delta\varphi_{rev} = \frac{RT}{F} \times \ln\left(\frac{P_{K^+}[K^+]_{cis} + P_{Cl^-}[Cl^-]_{trans}}{P_{K^+}[K^+]_{trans} + P_{Cl^-}[Cl^-]_{cis}}\right)$$ ....Equation 3

$$d = 0.5 \times \frac{G}{\lambda} + \sqrt{\frac{G^2}{4\lambda^2} + \frac{4GL}{\lambda\pi}}$$ ....Equation 4

2.2.1.3 Gating Model Analysis

One can quantify and analyze the voltage dependence of a channel with Boltzmann Equation under the following assumptions. First, equilibrium must be reached. For triangular voltage ramps, the change of voltage may be too fast to reach equilibrium. Therefore, an extrapolation of the parameter to zero frequency was used to mimic equilibrium situation. Second, a simple two-state (open and closed) model is used. With these assumptions, one can then use Boltzmann distribution to study the influence of voltages for channels [90].

$$\Delta E = nFV_0 - nFV = nF(V - V_0)$$ ....Equation 5

$$\frac{P_o}{P_C} = \frac{G - G_{min}}{G_{max} - G} = e^{-\frac{\Delta E}{RT}} = e^{-\frac{nF(V - V_0)}{RT}}$$ ....Equation 6

$$\ln \frac{G_{max} - G}{G - G_{min}} = \frac{nF}{RT}(V - V_0)$$ ....Equation 7

P_o and P_c here are the probability of the channels being in the open state and the closed state, respectively. G, G_{max}, G_{min} are the conductance at any voltage, the maximal conductance and the minimal conductance respectively. Here the n represents the number of charges translocate through the field upon gating. V_0 shows the voltage at which half of the channels in the ensemble are closed (or open) ($P_o/P_c = 1$). ΔE is the energy difference between open and closed state. nFV_0 is the energy difference in the absence of a membrane potential, whereas nFV is the voltage-dependent energy difference. With the help of these two parameters, one can then compare the voltage dependence between different channels

2.2.1.4 Statistical Analysis

Aggregate results are reported as means ± S.D. with the number of independent experiments indicated in parentheses. The symbol, N, is used to indicate the number of experiments performed with a specific protocol. Unless otherwise specified, the probability of observing the behaviors reported was 100%. Significant differences in values were tested using the Student's t test.

2.2.2 Purification Of Bax

The Bax protein was purified as reported previously [164]. The construct pTYB1-Bax was transformed into competent cells (E. coli strain BL21(DE3)pLysS), following the protocol from Agilent Technologies. Since pTYB1 is ampicillin-resistant, 100 µg/ml of ampicillin was used as a selection marker throughout the whole cell culture

procedure (until the cell pellets were harvested). The transformed BL21(DE3)pLysS cells were first allowed to grow on agar plates overnight at 37 °C. Cells from a few colonies were inoculated into 40 mL of Terrific Broth and grown at 37 °C, shaken at 200 rpm. When the culture reached an $O.D._{600}$ between 0.6-0.8, it was equally transferred to two 2 L flasks, each with 980 mL of Terrific Broth medium and shaken at the same rate and temperature. 1 mL of 1 M IPTG was added to each flask once the $O.D._{600}$ of the 1 L cultures reached 0.6-0.8 (final concentration of IPTG was 1 mM). IPTG here was used to induce the production of Bax. It works by mimicking lactose that releases the lac repressor from the DNA operator site upstream of the gene of interest (Bax here). Falling off of the lac repressor allows the target gene to be transcribed by T7 RNA polymerase. Three hours after the addition of IPTG, the cell culture was centrifuged at 5000 g, 4 °C, for 15 minutes (Beckman J-6B centrifuge). The cell pellets were resuspended with TEN buffer [20 mM Tris-HCl, 5 mM EDTA (disodium salt), 500 mM NaCl, pH 8.0] to bring up to a total volume of 60 mL (from 2 L culture). The resuspended cell pellets were frozen at -20 °C.

To harvest the protein, the pellets were thawed and the cells lysed with a French Press using 2 passes at 1000 psi. All the following steps were done at 4 °C. The lysate was centrifuged at 40000 rpm (about 100000 g, Beckman L8-70M ultracetrifuge, 50Ti rotor) for 30 minutes, to separate soluble proteins from inclusion bodies, membranes, etc. The supernatant was filtered with a 0.45 μm filter and then loaded onto a chitin column (NEB Inc.) with 3 mL of column volume (CV). Chitin beads were used here because they can bind to the intein engineered into the C-terminus of the Bax protein.

When first prepared, the chitin column was washed with at least 20 CV of double-distilled water at 1 mL/minute to remove the ethanol which was the original slurry. Then 20 CV of TEN buffer (20 mM Tris-HCl, 5 mM EDTA , 500 mM NaCl, pH 8.0) was applied at a flow rate of 1 mL/minute. Finally, the supernatant (soluble fraction of the cell lysate) was loaded onto the chitin column (flow rate = 1 mL/minute). Loosly bound material was washed out with 20 CV of a low EDTA TEN buffer (20 mM Tris-HCl, 1 mM EDTA , 500 mM NaCl, pH 8.0). The next step is to induce the self-cleavage of intein with the reducing agent DTT (30 mM DTT, 20 mM Tris-HCl, 1 mM EDTA, 500 mM NaCl, pH 8.0, prepared fresh), thus releasing Bax from the column. Three CV of the DTT solution applied at a 1- 2 mL/minute. The column was left to incubate with DTT for 48 hours for the cleavage reaction to take place.

Bax was eluted with 3 CV of low EDTA TEN buffer (1 mL/minute). The high salt (NaCl) and chelating reagent (EDTA) were removed by dialysis (cutoff = 4000-6000 kDa). The first dialysis was against 3 L of solution (10 mM Tris-HCl, 1 mM EDTA, adjusted to pH 8.0) overnight at 4 °C. A second dialysis was conducted against 5 L of solution [10 mM Tris-HCl pH 8.0] overnight . This final product was mixed with glycerol (final concentration 10%, v/v) and passed through a 0.22 µm filter to sterilize. Aliquots of 100 µL in glass tubes were frozen with an ethanol-solid CO_2 bath under rigorous shaking (shell-freezing). These aliquots were stored at < -80 °C.

The protein concentration was determined by the BCA assay (Pierce Chemical), and the results were typically 15-35 µg of protein/mL. Silver-staining (Thermo Scientific) following SDS/PAGE (12% gel) showed at least 95% monomeric Bax. Each aliquot was only thawed on ice right before an experiment.

CHAPTER 3: BAX FORMS TWO TYPES OF CHANNELS, ONE IS VOLTAGE-GATED

3.1 Abstract

The pro-apoptotic protein, Bax, when activated permeabilizes the mitochondrial outer membrane allowing the release of proteins into the cytosol and thus initiating the execution phase of apoptosis. When activated Bax was reconstituted into phospholipid membranes, we discovered a new property of Bax channels, voltage-gating. We also found that the same Bax sample under the same experimental conditions could give rise to two radically different channels: Type A: small, well-behaved, homogeneous and voltage-gated; Type B: large, noisy and voltage independent. One Type B channel can be converted irreversibly into a population of Type A channels by the addition of La^{3+}. This conversion process appears to involve a 2-dimensional budding mechanism. The existence of these two types of Bax channels suggests a process for controlling the degree of mitochondrial outer membrane permeabilization.

3.2 Introduction

Despite being a soluble cytosolic protein, Bax can undergo conformational changes to form transmembrane channels in the mitochondrial outer membrane, permeabilizing it and thus releasing a number of proteins, including cytochrome c, to trigger the execution phase of apoptosis. As a member in the Bcl-2 family of proteins, Bax plays a crucial role in promoting apoptosis. The Bcl-2 family proteins are characterized by having at least one of the four Bcl-2 homology domains (BH1-BH4). The consensus in the field is that there are three groups of proteins in the Bcl-2 family [165]: proapoptotic pore-forming (Bax, Bak), antiapoptotic (Bcl-2, Bcl-xL, etc), and the

proapoptotic BH3-only proteins (Bid, Bim, etc). Upon receiving proapoptotic signals, the BH3-only proteins, either directly [166–168] or indirectly [169,170] work on the pore-forming proteins to control the onset of apoptosis. This results in Bax monomers changing from being cytosolic proteins to oligomers in the mitochondrial outer membrane. Despite its obvious importance, the detailed mechanism of how this oligomerization occurs is still unclear. Questions like how monomeric Bax forms the active oligomer, what conformational changes Bax undergoes, how Bax interacts with other Bcl-2 family proteins, and many others are still under study. Due to the difficulties in solving the structure of membrane proteins in a membrane environment, many indirect ways have been taken to approach these questions [171–173], resulting in different models of the membrane structure of Bax oligomers. By using electron paramagnetic resonance (EPR), the spin-labeled reconstituted Bax was proposed to form dimers through the BH3 domain to nucleate the subsequent oligomerization [174]. Another group [175] found that Bax monomers first interact with each other through the BH1-3 domain, and this then triggers the conformational change of the rear pocket of Bax to cause further oligomerization. Experiments with mutants of Bax expressed in knock-out mice [176] indicated that only BH1 and BH3 are responsible for oligomerization in the membrane. These insights and others will eventually yield an understanding of the steps leading to the formation of Bax channels in the mitochondrial outer membrane [177,178]. Here we pursue a reductionist approach by examining the electrophysiological properties of channels formed by Bax in planar phospholipid membranes and thus gain insights into their permeability properties and dynamics.

Channels formed in a planar membrane system by Bax lacking the transmembrane domain were first studied in 1997 by Antosson *et al* [179] and Schlesinger *et al* [180]. The former group found that the channel activity was enhanced when negative potential was applied at the same side Bax added, indicating an intrinsically asymmetric channel formation. Under symmetric solutions of 125 mM NaCl, the conductance recorded showed elementary channels of 5.6 ± 0.2 pS increasing to 26 ± 7 pS, and then fluctuating between this level and 250 ± 25 pS [179]. The second group [180] reported Bax-induced conductances showing transitions among three different conductance levels: a closed state and two conductance levels. The experiments were performed in the presence of a salt gradient (450/150 mM KCl) and indicated an anion-selective conductance: $P_K/P_{Cl} = 0.32$ [180,181]. The Antonsson group reported a preference for cations: $P_{Na}/P_{Cl} = 2$. The conductance observed by Schlesinger and coworkers showed mild outward rectification in symmetrical 150 mM KCl along with rapid flickering at 70 mV and periodic closure at -70 mV.

Studies with full-length Bax in the same system reported the formation of conductances quickly followed by membrane instability (membranes usually ruptured after some tens of minutes, or even shorter when the concentration of Bax was around 1 nM, with voltage held at 40 mV) [182]. This led Basañez and coworkers to demonstrate that added Bax induces measurable instability in planar membranes, reducing their ability to withstand high voltages. They proposed that Bax induces the formation of lipidic pores and that these are responsible for the release of proteins from mitochondria.

Patch-clamping of mitochondrial membranes isolated from cells undergoing apoptosis or treated with Bax was used to study the electrophysiological behaviors of

channels presumably formed by Bax. Jonas *et al.* performed intracellular patch-clamping of squid mitochondria treated with Bax (both full length and truncated) and found that the conductance of the channels that were formed did not comprise multiples of a single unitary conductance and there was no consistent major conductance level [183]. Kinnally and coworkers recorded channels in mitochondria from cells undergoing apoptosis and called these mitochondrial apoptosis-induced channel (MAC). They provide compelling evidence that these are due to the presence of either Bax or Bak [184]. In symmetric media of 150 mM KCl, these MAC channels showed incremental steps around 300 pS that were voltage-independent, and cation-selective.

Here we report results using full-length Bax, activated with octyl-glucoside, reconstituted into planar phospholipid membranes. We found that Bax forms two types of channels with different characteristics. One of these is voltage-gated, closing asymmetrically at elevated potentials. Their properties and dynamics point to possible roles in the apoptotic process.

3.3 Materials and Methods

3.3.1 Materials

Diphytanoylphosphatidylcholine was purchased from Avanti Polar Lipids (Alabaster, AL). Cholesterol was from Sigma (St. Louis, MO). Asolectin (polar extract of soybean phospholipids) was generated from lecithin Type II-S (Sigma Chemical Co., St. Louis, MO) purified as described in [185]. Stock solutions of $LaCl_3$ used in these experiments were either 1 mM or 10 mM in distilled water.

3.3.2 Preparation of Bax

Recombinant full-length human Bax was made as previously described [31,164] and after elution from the chitin column (New England Biolabs Inc., Ipswich, MA) was dialyzed (12,000 MW cut-off) at 4 °C first for 24 hours against 3 liters of 1 mM EDTA and 20 mM Tris-HCl, pH 8.0 and then against 5 liter of 20 mM Tris-HCl, pH 8.0 for 48 hours. The Bax was then supplemented with glycerol to 10 % (v/v) and filtered sterilized through a 0.2 μm filter. Aliquots (generally 0.2 ml) were rapidly shell-frozen in ethanol and dry ice and stored at <-80 °C. The concentration of Bax was 10-35 μg/ml (depending on the preparation), determined by MicroBCA Protein Kit (Pierce Chemical Co.). SDS/PAGE was used to test the purity of protein and silver staining showed 95% of the stain in the monomeric Bax band. Due to its tendency to oligomerize over time in 4 °C [186], Bax was frozen immediately after purification and only thawed on ice right before use. No detergent was used in protein isolation or purification. To activate monomeric Bax, it was incubated with β-octyl glucoside of a final concentration of 0.7 % (w/v) for at least 30 minutes on ice. The concentrations of activated Bax indicated in this paper were based on the monomeric Bax (21 kDa) since the activated form is heterogeneous.

3.3.3 Electrophysiological Recordings

Planar membranes were formed by the modified monolayer method [159,160], across a hole (diameter of 100 μm) in a Saran partition after coating with petrolatum. For most experiments the membrane-forming solution, composed of 0.5% (w/v) DPhPC, 0.5% (w/v) asolectin, 0.05% (w/v) cholesterol in hexane, was layered on the surface of the aqueous solution contained 1.0 M KCl, 1 mM $MgCl_2$, and 5 mM PIPES

pH 6.9. For selectivity experiments the concentration of KCl was reduced to 0.1 M on the grounded side. Reversal potentials were measured and permeability ratios calculated using the Goldman-Hodgkin-Katz equation [161,187]. After hexane evaporation and monolayer formation, the membrane was formed. Calomel electrodes with saturated KCl bridges were used to interface with the aqueous phase. The voltage was clamped and the current recorded. In the text, we specify the number of experiments performed in which the particular observation was made. If all the experiments yielded the same outcome, only the number of experiments is indicated. If only a subset of experiments yielded that result then we also specify the total number of experiments performed.

3.3.4 Calculation of Channel Diameter

Single-channel conductance measurements were converted to estimates of channel diameter as follows:

$$d = 0.5\frac{G}{\lambda} + \sqrt{\frac{G^2}{4\lambda^2} + \frac{4GL}{\lambda\pi}}$$

where d is the diameter of the channel; G is the conductance; λ is the conductivity; L is the length of the channel (5 nm). This calculation assumes that the conductivity of the solution in the channel is the same as that of the bulk phase. The equation takes into consideration the access resistance as previously described [163].

3.4 Results

Addition of full-length Bax into the aqueous phase of a planar phospholipid membrane (final concentration of Bax, about 10 nM) under voltage-clamped conditions

results in one of two different types of conductance behavior (see details below). These are designated as Type A and Type B. The probability of the occurrence of Type A and Type B is around 50%. In most experiments, only one of the two types was observed. In very rare cases (the probability is less than 5%), we observed a spontaneous change from Type A to Type B channels after new additions of Bax (but not vice versa).

3.4.1 Type A

There are basically four characteristics for Type A behavior: (1) discrete, low current-noise increments of conductance representing channel formation, (2) voltage-gating, (3) no change in conductance or voltage-gating after addition of $LaCl_3$ (as opposed to the changes seen with Type B). After the addition of activated Bax, the conductance increased in discrete and step-wise increments, with virtually no decrements (Fig. 3.1). These conductances had very low current noise in comparison with the Type B channels (*vide infra*). The total conductance achieved ranged from a few to 100 nS, depending on the number of channels formed. The histogram of the insertion steps (Fig. 3.1 inset) appears to consist of three groups of conductances. These were fitted to three overlapping Gaussian curves. The fundamental unit seems to be the first Gaussian with a peak at 1.5 ± 0.4 nS. The peak of the second distribution

at 4.1 ± 0.7 nS has a conductance about 3 times as great, hinting at the simultaneous insertion/formation of three units. The third peak is twice the second.
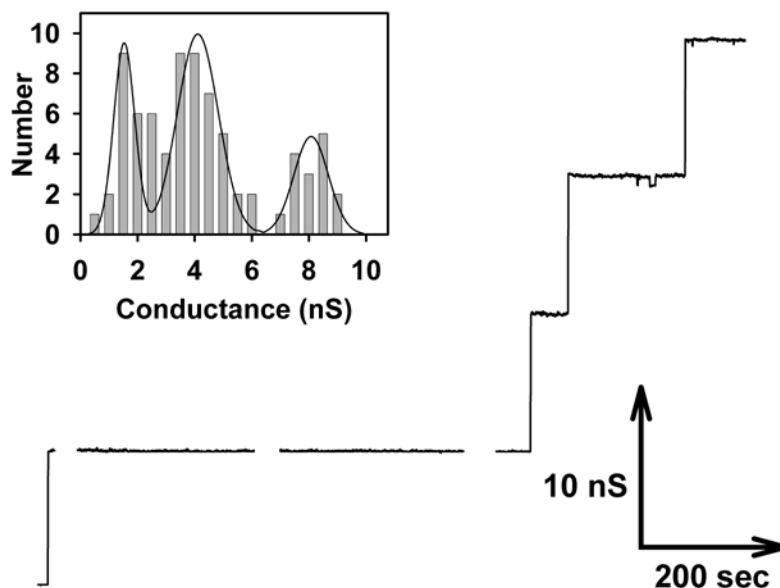

Fig. 3.1 Step-wise formation of Type A Bax channels. The membrane conductance increased (starting from 0 nS) as a function of time following the addition of octylglucoside-activated Bax to the aqueous phase (1.0 M KCl on both sides of the membrane). The transmembrane voltage was clamped at 10 mV. The solution was stirred during the breaks in the record. The histogram of conductance increments from 16 separate experiments is shown in the inset. Only a few steps were larger than 10 nS and not shown here for clarity. The histogram was fitted to three Gaussians with the following means and standard deviations: 1.5 ± 0.4, 4.1 ± 0.7, 8.1 ± 0.6.

Type A Bax channels are voltage-gated. When the transmembrane voltage was raised above 60 mV, a population of uniform, low-noise step-wise drops in conductance was observed (Fig. 3.2). The histogram of these events shows a single peak at 1.4 nS (Fig. 3.2 inset), matching the value of the first peak in the insertion histogram. This indicates that the membrane conductance was due to many virtually identical channels. Reducing the voltage to 10 mV results in slow channel reopening (Fig. 3.3) and the rate of reopening slows further the longer the channels are closed.
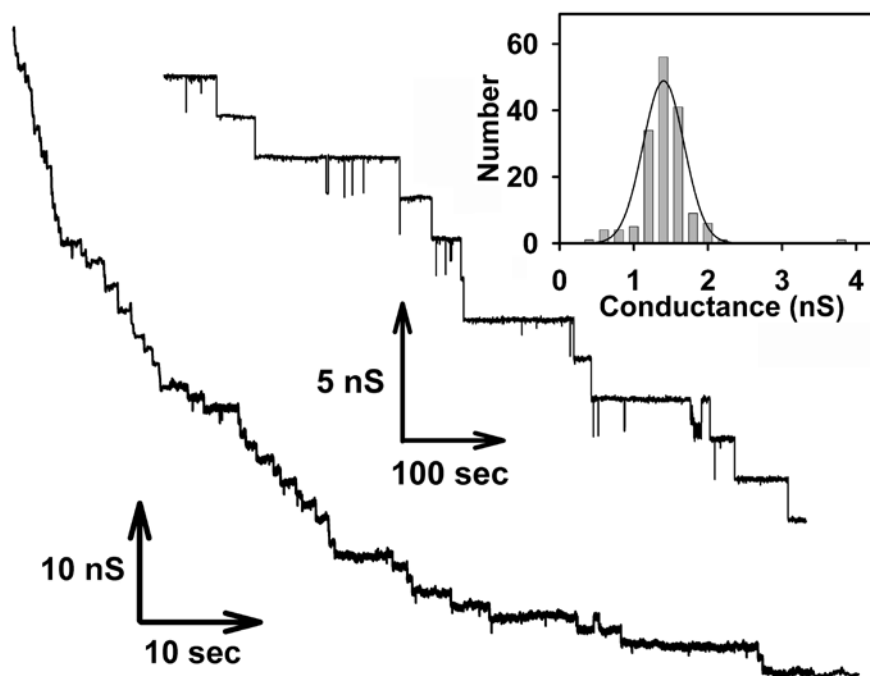
Fig. 3.2 Voltage-gating of Type A Bax channels. Stepwise conductance decrements were observed following the application of high voltage. (a) An example of an experiment with many Type A channels present in the membrane. The voltage was clamped at 70 mV. (b) An example of an experiment with fewer channels with voltage held at 60 mV. The inset shows a histogram of the conductance decrements observed in 10 separate experiments (1.0 M KCl on both sides of the membrane). This distribution has a mean ± S.D. = 1.4 ± 0.3.

The slow kinetics and adaptation to the applied voltage do not allow the system to reach

an equilibrium that would allow quantitation of the voltage-gating parameters.

In agreement with the Bax channels previously observed [179], the Type A

channels are asymmetric because they only closed when the voltage of one sign was

applied. The sign of the high voltage that could induce the drops in conductance varied

from experiment to experiment with a frequency of positive: negative = 13: 2. Thus in

most experiments the application of a positive potential on the side of the membrane to

which Bax was added resulted in channel closure exclusively at positive potentials,

demonstrating that all the channels were oriented in the same direction. This indicates

that the channels are forming in a cooperative and oriented manner reminiscent of the

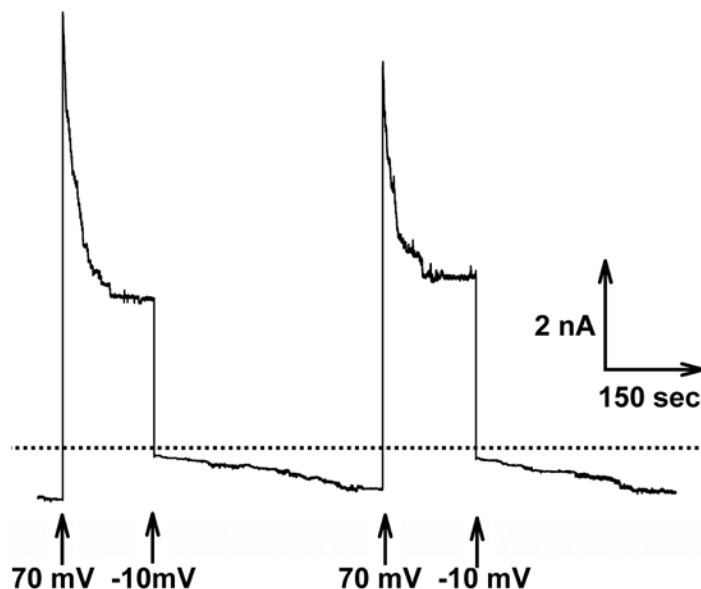"auto-directed insertion phenomenon" first described for VDAC channels [188].

Fig. 3.3 The slow kinetics of voltage-gating of Type A Bax channels. Bax channels wre formed in a planar membrane under a -10 mV potential (the dotted line is the zero current level). Channel closure occurred when the voltage was switched to 70 mV. The channels reopened slowly when the voltage was returned to -10 mV but reopening was not complete in the time allotted. This is evident in the lower level of the instantaneous current recorded following the application of 70 mV for the second time. Again channel closure occurred at 70 mV and reopening at -10 mV. The opening and closure is reversible but with slow kinetics.

Addition of La^{3+} to the medium had no effect on the conductance or on the

voltage dependence of the channels. This is important when considering the influence

of La^{3+} on the Type B channels. Thus characteristics of discrete, low-noise

conductance increments and voltage-dependent channel closure define what we refer

to as "Type A Bax channels".

3.4.2 Type B

In contrast to Type A, experiments that produced Type B conductance were

characterized by indistinct conductance increases that included a great deal of current

41

noise but were punctuated by some discrete increases of variable conductance. The

conductance increased to a total value from 60 to a few hundred nS before stabilizing.

Even after stabilizing the conductance fluctuated and continued to have excess current

noise (Fig. 3.4A). Unlike Type A, Type B conductance is voltage-independent (Fig.

3.4A) at both positive and negative potentials. Transmembrane voltages as high as 120

mV were applied without detecting any significant decrement or increment of

conductance in these Type B experiments. These characteristics define the behavior of

what we call "Type B Bax channels". Since Type B channels are voltage-independent,

there is no indication from these experiments as to whether the constituents of the

conductance in Type B experiments are due to many or just a single, huge channel.
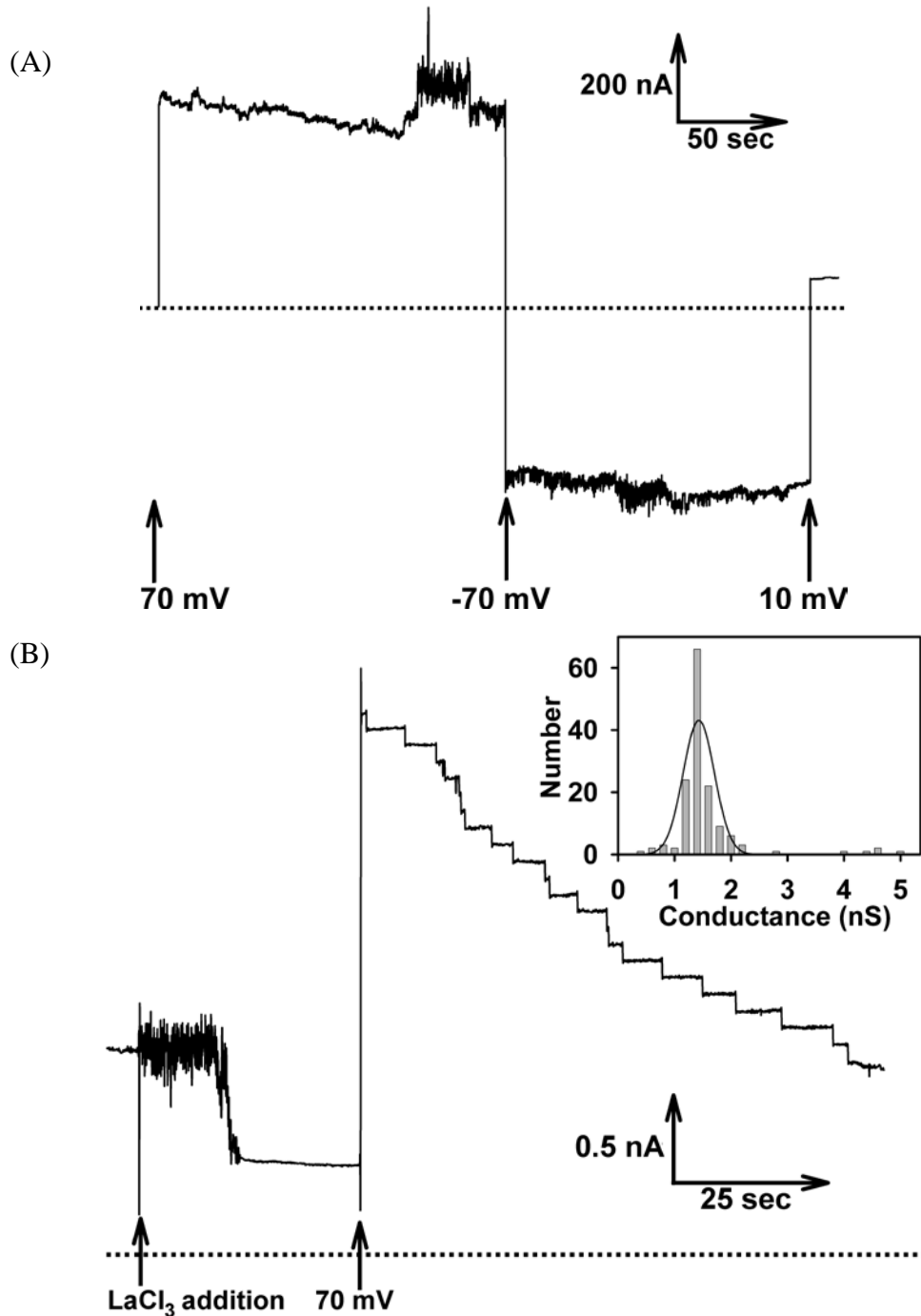
Fig. 3.4 Conversion of a voltage-independent Type B Bax channel into a population of Type A channels. **(A)** Addition of Bax resulted in a noisy conductance increase. Neither +70 nor -70 mV caused any significant decrement in conductance. **(B)** The voltage was held at 10 mV before 70 mV was applied as indicated. The addition of $LaCl_3$ (8 μM) to this same membrane resulted in a conductance drop by a little more than half. The large fluctuations were due to the stirring motor. Application of 70 mV resulted in a population of uniform-sized, step-wise decrements. The inset is a histogram of conductance decrements collected from 5 separate experiments performed in the same way. The histogram was fitted to a Gaussian with mean $\pm$ S.D. $= 1.4 \pm 0.3$. The dotted line designates the zero current level.

3.4.3 Conversion from Type B to Type A

It has been shown that lanthanides can act on membranes to change the surface potential and lateral pressure. They can induce membrane fusion and regulate certain membrane channels [189–193]. $LaCl_3$ affects Type A and Type B differently. $LaCl_3$ was added after the level of the conductance had reached a nearly constant value. It was added to the same side of the chamber to which Bax had been added so as to a final concentration of a few µM. Type A Bax channels showed neither a change in conductance (n=12), nor a change of the voltage-gating behavior (n=4) after $LaCl_3$ addition. However, for the Type B Bax channels $LaCl_3$ addition resulted in a huge drop (85% ± 15% of original level) of conductance (Fig. 3.4B). The drop was preceded by a variable delay time (8-113 sec, n=14) (Fig. 3.5), characteristic of a stochastic process. Moreover, the residual conductance after the drop showed voltage-gating (n=9 out of
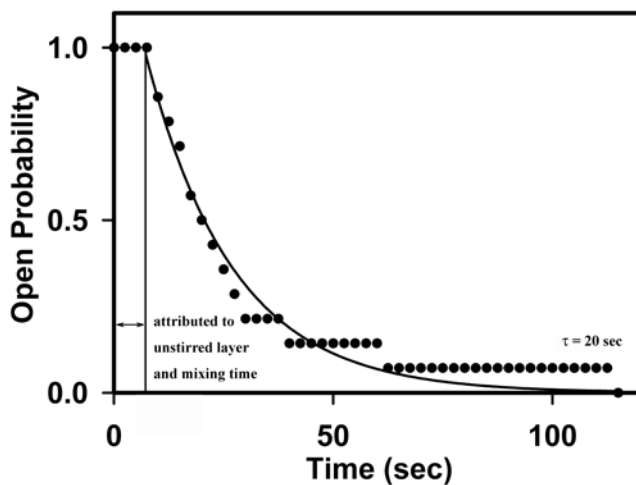
Fig. 3.5 Summary of the time delay between the addition of LaCl₃ and the beginning of the drop of conductance. Each data point represents the fraction of experiments in which the conductance had not started to decrease at the specified time (the x axis) following $LaCl_3$ addition. Data were collected from 14 experiments. Only one experiment was performed in the presence of a KCl gradient (*cis* = 1.0 M, *trans* = 0.1 M), and this had a delay time of 10 seconds. All others were with 1.0 M KCl on both sides. The fitted line has a time constant 20 seconds. The delay before the decay, attributed to the combination of diffusion time through the unstirred layer and time for mixing $LaCl_3$ into the solution, was 6.8 sec.

10) indistinguishable from the voltage gating of Type A Bax channels. Analysis of the step size of the decrements of the residual conductance under high voltage (Fig. 3.4 inset) shows the same pattern as that of *de novo* Type A (Fig. 3.2 inset). The stochastic behavior is consistent with a single large channel but the residual conductance is composed of many channels. Therefore, we propose a hypothesis that $LaCl_3$ helps to convert Type B into Type A Bax channels by a budding process. In analogy to vesicle budding from a membrane surface, a Type B channel undergoes lateral budding in 2 dimensions into many Type A channels.

The budding hypothesis is supported by a number of experimental and theoretical considerations. The stochastic delay prior to the conductance drop indicates that the drop involved a single structure, a single channel. Perhaps this single structure could have been present along with Type A channels, the latter obscured by the properties of the former. However, the complete lack of voltage dependence is inconsistent with this alternative. Despite the "noisy" record, the voltage dependent closure of Type A channels should have been detected. The La^{3+}-induced conductance drop did not have any detectable structure; i.e. there was no evidence of discrete closing events (n=14). A budding process would not be expected to result in discrete conductance drops, rather a more fluid reduction in conductance. Finally, calculations using the conductance prior to La^{3+} addition, assuming one large channel, resulted in a circumference that that was greater than the sum of the circumferences of the channels making up the residual conductance (n=13). This is consistent with the budding hypothesis if some of the protein making up the circumference of the large channel formed the Type A channels and some left the channel structure. The conversion of

45

Bax protein into non-conducting structures was evident in one experiment where the La^{3+}-induced conductance drop resulted in no residual conductance.

3.4.4 Measurement of the Selectivity of Type A Channels

The selectivity (P_K/P_{Cl}) of Type A Bax channels was determined in the presence of a gradient of KCl across the planar membrane (0.1M and 1.0M).   The permeability ratio was 3.6 ± 0.3 (mean ± S.D.) and did not change after $LaCl_3$ (3.7 ± 0.5) addition (n=5) (Table 3.1). La^{3+} must not be binding in a region of Bax that is close to the ions flowing through the membrane. Also, by monitoring both selectivity and conductance at the same time, it is clear that the selectivity did not change with conductance increments or decrements (n=5) (Table 3.1). This supports the conclusion that Type A Bax channels do not merge with each other to form larger channels.   All attempts to measure the selectivity of Type B channels failed, presumably because the Type B channels are unstable in the presence of an ion concentration gradient.

Before La³⁺	*After La³⁺*	*P value*
-24 ± 1.5 mV	-24 ± 2.2 mV	0.96
Low Conductance	*High Conductance*	*P value*
-24 ± 1.5 mV	-24 ± 1.8 mV	0.21
Early Time	*Late Time*	*P value*
-25 ± 1.4 mV	-24 ± 2.0 mV	0.10

Table 3.1: Lack of variation in reversal potential with time, conductance and La^{3+} addition. The reversal potentials of 5 separate Type A channel experiments were measured throughout the experiment, grouped, and compared to see if there were any distinguishable changes in channel selectivity before or after La^{3+}, between low or high conductance, and between the first half and second half of the experiment. Measurements were made in the presence of a KCl gradient (*cis* = 1.0 M, *trans* = 0.1 M) with the sign referring to the high salt side. Values are averages ± standard deviation.

3.5 Discussion

The reconstitution of full-length Bax, isolated in a functional manner from the soluble fraction of a bacterial lysate, into phospholipid membranes resulted in the formation of one of two types of channels. Type A is functionally homogeneous, with a distinct membrane orientation and with a single voltage-gating process. The voltage-gating resulted in channel closure at one sign of the membrane potential, depending on the orientation of the population of channels. These channels show weak cation selectivity and a conductance consistent with a pore diameter of 0.9 nm. Type A channels are unlikely to be able to translocate proteins across membranes.

The voltage-gating exhibited by the Type A channels is complex. Some of the complexity is attributed to kinetic delays as is evident in the slow reopening process (Fig. 3.3). The system did not reach an equilibrium during the time of the experiment and thus could not be fitted to a Boltzmann distribution. Thus the typical voltage gating parameters, n and V_0, could not be obtained. Furthermore, we suspect that closure is accompanied by some form of de-oligomerization because channel reopening following voltage-dependent closure becomes incomplete if the high closure voltage is maintained for extended periods of time.

Type B channels seem to be large channels, likely protein permeable. Their conductance fluctuates with time, and they are voltage-independent. These channels seem to be unstable in the presence of an ion gradient and are rapidly converted to Type A channels following the addition of La^{3+} by what appears to be a process of channel budding in 2-dimensions. The delay prior to budding is stochastic, characteristic of a

47

single structure undergoing the process. The transition has a time constant of 20 sec (n=14), consistent with an energy barrier of 80 kJ/mole.

The results reported here show some similarity with publications from other groups [179–181,184], but also major differences. No one else has yet reported the large uniform populations of channels reported here. Previous publications reported conductance changes in the range of the conductance increments observed here for the insertion steps, when corrected for differences in salt concentration, but those channels had much higher flickering rates. There has been no report of voltage-gated channels formed by Bax, although the voltages applied by others have been up to 50 mV [184], perhaps insufficient to observe significant channel closure. As for the selectivity, our measurements are similar to those of a previous study for mitochondrial apoptosis-induced channel (MAC) [194], slightly more cation-selective than reported by one group for channels formed by truncated Bax [180], but opposite to the value observed by another [180] (anion-selective in this publication). Possible reasons for the differences (see also Westphal *et al.* [177]) are: (1) Bax may form different structures under different conditions; (2) the use of full-length vs. truncated Bax; (3) the quality of the Bax including mode of isolation and storage. The Bax used in the present work was shown to be functional by testing its channel-forming ability on isolated mitochondria. When activated either by detergent or tBid, the activated Bax permeabilized the mitochondrial outer membrane to proteins [31].

The paucity of structural information makes it difficult to compare the channels reported here to those formed in isolated mitochondria. Evidence indicates that helices α5, α6, and α9 of Bax are responsible for membrane insertion [174,195,196]. Several

possible models of active Bax oligomers in membrane have been reported. For example, it has been proposed that the BH3 domain of Bax, upon being activated by BH3-only proteins, binds to α1/α6 pocket of a second Bax monomer, and this activation propagates to other monomers resulting in oligomerization [178]. Others have provided evidence for a "two interface" model wherein oligomerization occurs through two interacting surfaces: BH3:groove and α6:α6. Bax monomers first form dimers through a BH3 domain on one protein binding to the BH3-binding groove of another protein. The dimer now has two α6 helix regions and is therefore a divalent ligand. These oligomerize by binding to each other via their α6 helix domains [174,177]. At present there is insufficient evidence to come to a clear consensus. There is also no clear consensus on the number of Bax monomers forming the active structure, it varies from 4 [197], 9 [184], or even larger than 100 [198]. The reported size of the channels also varies from a few to around 27 nm depending on the system studied [166,197–199]. Perhaps that is the nature of the Bax pore. The variable size of the Type B channel would be consistent with a variable number of Bax monomers forming the channel.

The histogram of conductance steps of voltage-gated closures of Type A channels (Fig. 3.2 inset) has a peak at 1.4 nS and this is the same as the first peak of the insertion histogram (Fig. 3.1 inset). Higher conductance insertion events may represent the simultaneous insertion/formation of multiple channels at once. The sizes of these channels can be calculated assuming cylindrical structures whose internal conductivity is the same as the bulk phase. The 1.4 nm decrements of Type A channels correspond to a diameter of 0.9 nm. This is smaller than the size of cytochrome c (around 3.4 nm), the smallest protein released from mitochondria following Bax insertion into the outer

membrane. However, from the stochastic delay prior to transformation of Type B into Type A, each Type B conductance should be due to one structure, likely one channel. Although variable in conductance, if formed by cylindrical channels these would be very large (up to 40 nm), very suitable for protein translocation. As for which domains of the Bax molecules are responsible for the voltage-gating, combining the previous models [174,175], it could be the charged residues on helix α5, which is transmembrane.

One can only speculate on the physiological relevance of our results. The instability of the Type B channels and conversion to Type A may indicate the presence of a regulatory mechanism. The ability of Bax channels to release proteins would be unstable, easily converted to protein-impermeable channels in response to an appropriate signal. This would not be La^{3+} but some other agent acting in a similar manner. Lanthanides inhibit the stretch-dependent opening of stretch-sensitive channels by acting on the membrane lipids and affecting the membrane tension. A similar action may be the trigger that causes the Type B channels to convert to Type A. The function of the voltage dependence is unclear although highly-conserved voltage gated channels, the VDAC channels, are found in the all mitochondria tested. The mitochondrial outer membrane potential has been measured at around 30~40 mV [200–202], and theoretically it could increase to 60 mV [200]. In addition local electric fields, such as those resulting from surface charge, could act of the voltage sensor of the Type A channels resulting in closure or channel disassembly. The physiological role, if any, of the asymmetrical orientation of Type A channels is unknown. However, according to Ausili *et al.* [203], the orientation of the C terminal of Bax can be influenced by the lipid environment. Hence the cooperative and variable orientation may serve some

function such as responding to the changing lipid composition of the outer membrane during apoptosis. Regardless, the reductionist approach used here has identified novel properties of Bax channels that will provide insight into the structure and function of these channels.

3.6 Acknowledgements

CHAPTER 4: **BAX CHANNEL TRIPLET: COOPERATIVITY AND VOLTAGE GATING**

4.1 Abstract

Bax, despite being a cytosolic protein, has the distinct ability to form channels in the mitochondrial outer membrane capable of releasing proteins that initiate the execution phase of apoptosis. When studied in a planar phospholipid membrane system full-length activated Bax can form conducting entities consistent with linearly organized three-channel units displaying steep voltage-gating (n=14) that rivals that of channels in excitable membranes. In addition the channels display strong positive cooperativity possibly arising from the charge distribution of the voltage sensors. Based on the functional behavior, one of the channels in this functional triplet is oriented in the opposite direction to the others often resulting in conflicts between the effects of the electric field and the positive cooperativity of adjacent channels. The closure of the first channel occurs at positive potentials and this permits the second to close but at negative potentials. The closure of the second channel in turn permits closure of the third but at positive potentials. Positive cooperativity manifests itself in a number of ways including the second and the third channels opening virtually simultaneously. This extraordinary behavior must have important although as yet undefined physiological roles.

4.2 Introduction

Voltage-gated membrane channels are proteins that have evolved to be especially sensitive to changes in membrane potential. They contain a voltage sensor whose movement is coupled to the conformational state of the protein which, in turn, determines the functional state of the channel: open or closed. Voltage-gated channels

are mostly studied in cells that possess electrical excitability: muscles and neurons [72,78]. However, these are also found in other cell types (e.g. osteoblasts [204], endocrine cells [205], dynoflagellates [206], and bacteria [207]) and in intracellular membranes (e.g. tonoplasts [206], mitochondria [208]). Bax is a small (21.2 kDa) soluble cytosolic protein [164] that can be activated by pro-apoptotic signals, through an as yet unclear mechanism, to insert into the mitochondrial outer membrane to form membrane channels large enough to allow proteins to translocate [166,168,174]. Thus Bax is one of the killer proteins in the apoptotic process, initiating the execution phase of apoptosis. In addition, Bax can also form highly ordered, relatively small voltage-gated channels in phospholipid membranes [209]. Here we report that these channels show an unprecedented level of cooperativity and a steepness of voltage dependence that rivals that of the voltage-gated channels responsible for the electrical excitability of neurons and muscle cells.

Antonsson *et al.* [179] and Schlesinger *et al.* [180] were the first groups to study Bax channels on planar membranes using truncated Bax (BaxΔC19) and observed a variety of discrete changes in conductance interpreted as single channels. Rectification and changes in channel activity were observed when different voltages were applied. Later similar results were reported for full-length Bax [210]. Channels observed in mitochondria undergoing apoptosis (mitochondrial apoptosis-induced channel, MAC) were attributed to Bax [184]. In all these experiments, including those with MAC, no voltage gating was reported in the range of ±50 mV. Using improved techniques for handling Bax, we discovered that full-length Bax can form two types of channels (Type A and Type B), and one of them (Type A) is voltage-gated [209]. In 1.0 M KCl, Type A Bax channels have fundamental conductances of 1.5 ± 0.4 nS and 4.1 ± 0.7 nS, with the

54

latter about 3 times of the former. Upon the application of high positive voltages on the side of Bax addition, Type A channels close in a series of uniform decrements (1.4 ± 0.3 nS). We now show that these have a preference for being organized into a triplet of channels with different functional properties.

The existence of double-barreled [211] and triple barreled channels [212] are well known but the triplets formed by Bax have an unprecedented combination of mixed orientation, cooperativity and very steep voltage gating. Indeed, different functionalities are observed depending on how the voltage is applied. A constant 70 mV potential results in closures of 3 individual channels in a manner similar to what was reported for a population of seemingly identical Type A channels. However, the application of voltage ramps allowed us to discover striking differences between these channels of indistinguishable conductance. Each channel has different voltage gating properties, responding to potentials of opposite sign, and together they show remarkable cooperativity. The cooperativity and voltage gating often conflict resulting is complex responses to time-dependent voltage changes. From these properties, we deduce a model of their structure and interaction consistent with all observations.

4.3 Materials and Methods

4.3.1 Materials

Phospholipids were obtained from Avanti Polar Lipids (Alabaster, AL). Cholesterol was purchased from Sigma (St. Louis, MO).

4.3.2 Preparation of Bax

Recombinant full-length Bax was purified as previously published [164,209]. Only the soluble protein was recovered from the bacterial lysate leaving, any inclusion bodies behind. The soluble proteins was affinity purified by means of a self-cleavable intein tag. Glycerol was added (10% v/v) and then the solution shell-frozen in 100 μL aliquots in thin glass tubes using ethanol/dry ice and stored at < -80°C. Silver-staining following SDS-PAGE showed at least 95% monomeric Bax. The concentration of Bax was typically 15-35 μg protein/mL. Each aliquot was only thawed on ice right before an experiment.

4.3.3 Electrophysiological recordings

Planar phospholipid membranes were formed by the monolayer method [159,160]. The monolayers were formed by layering the lipid solution (0.5% (w/v) DPhPC, 0.5% (w/v) asolectin (polar extract of soybean phospholipids), and 0.05% (w/v) cholesterol in hexane) on the surface of the aqueous solutions (1.0 M KCl, 1 mM $MgCl_2$, and 5 mM PIPES, pH 6.9) on either side of the partition. The membrane was formed across a 0.1 mm hole in the partition. Calomel electrodes were used to interface with the aqueous phase. The membrane voltage was clamped using a high-quality operational amplifier in the inverted mode and the current recorded using Clampex 10.3 software. Data was generally low-pass filtered at 500 Hz but in some experiments this was reduced to 5 kHz. Typically 20-50μL of activated Bax was dispersed in 5mL aqueous solution on one side of the membrane. Bax was activated by exposing it to 1% (w/v) of β-octyl-glucoside for at least 30 minutes on ice [213,214]. No channel-forming activity was

detected without this activation and addition of only the β-octyl-glucoside did not produce any channels.

All experiments reported were performed on Type A Bax channels. Around half of the experiments performed yielded Type A channels, the rest were Type B. Type A channels are voltage-gated and display a low level of current fluctuation, other than gating. Type B channels are not voltage-gated and have a much higher level of current noise. Voltage ramps were applied to investigate the behavior of these channels and determine their voltage-gating parameters. All the results reported were observed in at least 3 independent experiments, with usually multiple repeats of the illustrated behavior within each experiment.

4.3.4 Quantification of voltage dependence

The Boltzmann distribution was used to determine the parameters of voltage dependence.

$$\frac{P_O}{P_C} = e^{-\frac{\Delta E}{RT}}$$

$$\Delta E = nFV_0 - nFV = nF(V - V_0)$$

$$\ln(\frac{G_{max} - G}{G - G_{min}}) = \frac{nF}{RT}(V - V_0)$$

where P_O and P_C are the probability of the channels being in the open and closed state, respectively. ΔE is the energy difference between open and closed state. nFV_0 is the energy difference in the absence of a membrane potential, whereas nFV is the voltage-dependent energy difference. n is the number of charges that would need to move across the entire electric field to account for the voltage dependence, and V_0 is the voltage at which half of the channels on the membrane are open. G, G_{max}, and G_{min} are

the conductance at any voltage, the maximal conductance and the minimal conductance, respectively (Fig. 4.1). An important condition for using the Boltzmann distribution is that the distribution is determined at equilibrium. When using voltage ramps, the rate of change in voltage may be too fast to allow the system to reach equilibrium. Therefore, we determined the value of "n" at various rates of voltage change and extrapolated the fitted line of the n vs. rate plot to zero rate in order to estimate the value of 'n' at equilibrium. For single-triplet experiments, we averaged the current
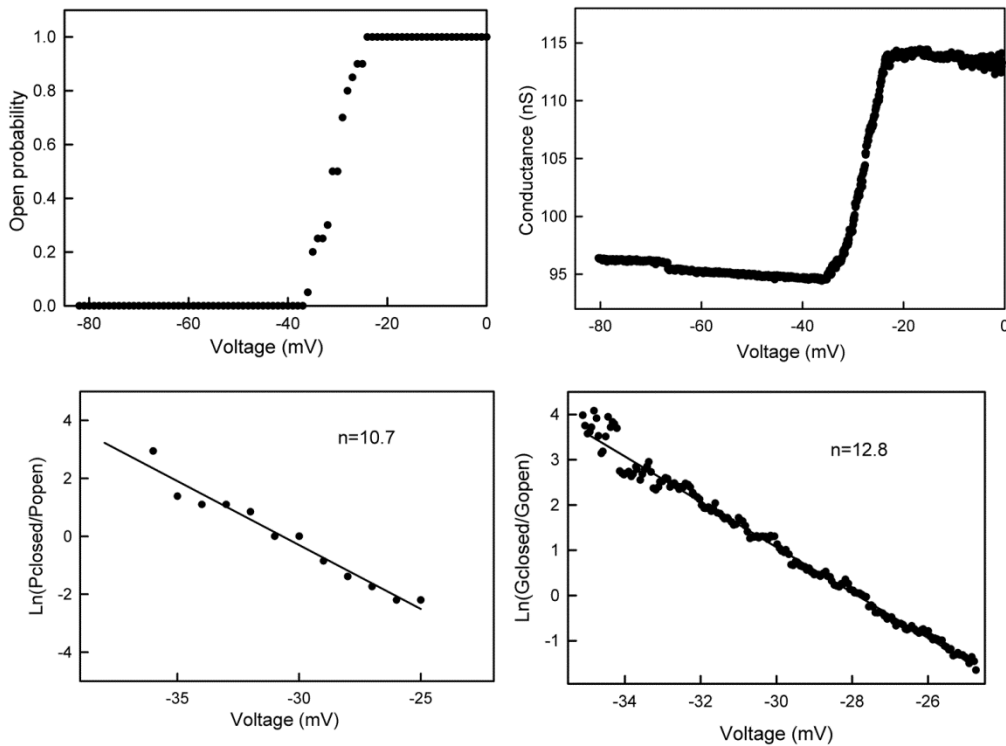
Fig. 4.1 Samples of the analysis used to obtain the steepness of the voltage dependence of the gating process.
Upper left: The data was collected from an experiment with a single triplet. The portion of 20 consecutive records of the current response to a 30 mHz triangular voltage wave (±82mV) were analyzed to determine the probability of finding channel ② open as the voltage declined from 0 to -82 mV. This is the channel closing process. This data was log transformed as described in Methods to yield the lower left panel. The line is the least squares fit through the data. From the slope of the line, the steepness of the voltage dependence, n, and V_0 were determined and the n values are indicated. The right panels are similar except that in this experiment the membrane contained many triplets (perhaps 28) only some of which were gating. The triangular wave was run at 9 mHz (±80mV).

58

records from at least 20 consecutive triangular ramps and for multi-triplet experiments, we averaged the records from at least 5 ramps to obtain valid parameters. The use of voltage steps to collect data for conductance voltage curves is problematic for large channels because keeping the channel at a fixed voltage for some time results in time-dependent adaptation to the voltage which differs from one voltage level to the next, degrading the information that is obtained.

4.3.5 Statistical analysis

Aggregate results are reported as an average ± one standard deviation with the number of independent experiments indicated in parentheses. The symbol, N, is used to indicate the number of experiments performed with a specific protocol. Unless otherwise specified, the probability to observe the behaviors reported here when we tested the protocols is 100%. Significant differences in values were tested using the Student's t-test.

4.4 Results

The dispersal of activated full-length Bax protein (21.2 kDa) in the aqueous phase next to a phospholipid membrane results in increases in permeability, characteristic of the formation of membrane channels. Of the two types of channels that form [209], one (Type A), is highly ordered (30 experiments, 59% of all experiments). As expected for channels, the permeability formed is a multiple of a fundamental unit, 4.5 nS (Fig. 4.2). What is unusual is that this unit has properties consistent with a triplet of channels (designated channel ①, ② and ③) that are highly cooperative and voltage gated (70
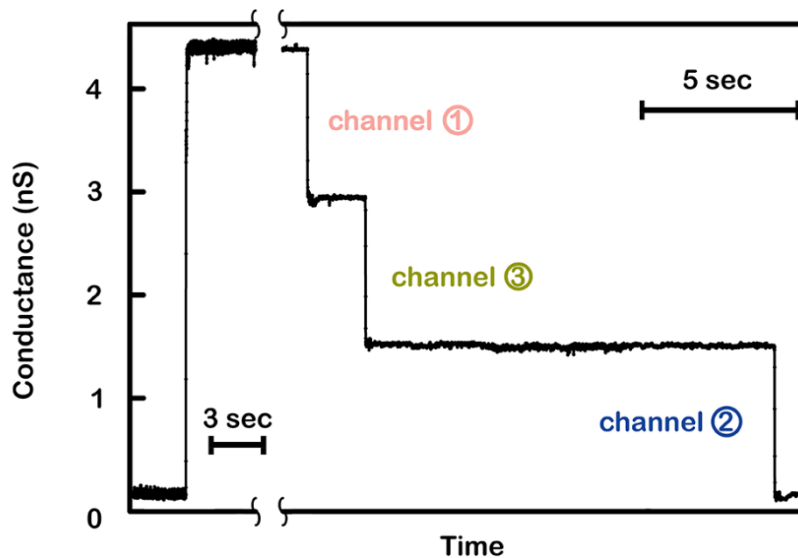
Fig. 4.2. Formation of highly ordered, voltage-gated Type A Bax channels in a planar phospholipid membrane. Formation of a single unit (left, N=7, 23% of all Type A experiments) under a 10 mV potential followed by three conductance drops when a 70 mV potential was applied (right). The proposed order of closure (channel ①, ③ then ②) is based on the model presented in Fig. 4.12.

mV was applied after the break in Fig. 4.2). Each channel in the triplet is likely an oligomer of Bax. The formation of the permeability occurs rapidly even for a multiunit event (Fig. 4.3). The 110 nS permeability formed within 2 msec. As previously reported, the application of a constant voltage results in stepwise conductance decrements (Fig. 4.4) consistent with the closure of individual channels and the simplest explanation would be that a population of identical channels inserted together perhaps as a preformed aggregate or crystal. However, further analysis reveals complex properties. The application of 7.38 mV/sec voltage ramps to a single conductance unit (4.4 nS in this case) shows the total absence of voltage gating for several cycles. Remarkably, following a single conductance drop of 1.5 nS, gating was evident in ALL 90 subsequent ramp cycles performed in that experiment (Fig. 4.5 only shows the first 4).
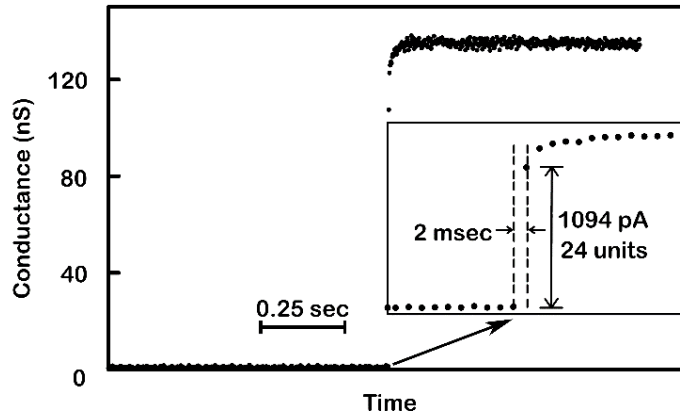
Fig. 4.3 Formation of highly ordered, voltage-gated Type A Bax channels in a planar phospholipid membrane. There is near simultaneous formation of many Bax channels under a 10 mV potential. Inset expands the region of formation/insertion showing an increase in current from 0 to 1094 pA within 2 milliseconds. There is a further slower increase for tens of milliseconds. Assuming that each conducting unit is 4.5 nS (from Fig. 4.2), 24 units formed within 2 msec. This is one of 23 multi-channel experiments, 77% of all Type A experiments.
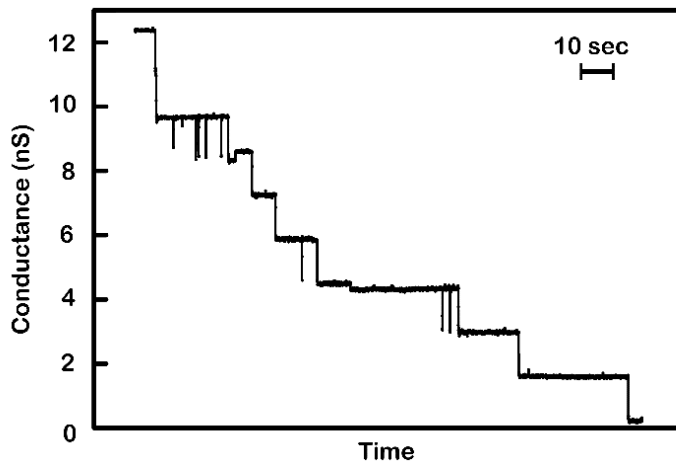
Fig. 4.4 Application of 70 mV resulted in 9 conductance decrements, equivalent to the closure of all the channels in 3 conducting units. This is typical of 36 experiments.

The first conductance drop (channel ①) occurred at a high positive potential (98 mV for the example shown in Fig. 4.5, 86 ± 14 (5) mV), consistent with experiments in which a constant voltage was applied. The subsequent gating (channel ②) took place at negative voltages ($V_0 = -27 \pm 4$ (4) mV for 7.38 mV/sec ramps) with reopening taking place as the potential became more positive. Thus the gating took place between 2.9

61

and 1.5 nS consistent with gating of only channel ②. The average values of these

intermediate conductance levels from 5 experiments are: 2.93 ± 0.06 and 1.45 ± 0.13

nS (Fig. 4.6). The closure of channel ② not only occurred at each subsequent cycle

but it occurred within a very narrow voltage range, indicating a high steepness of

voltage dependence (Fig. 4.7). This pattern of gating was highly reproducible and was

evident both in membranes with a single 4.5 nS unit conductance and those with many

units (Fig. 4.8).
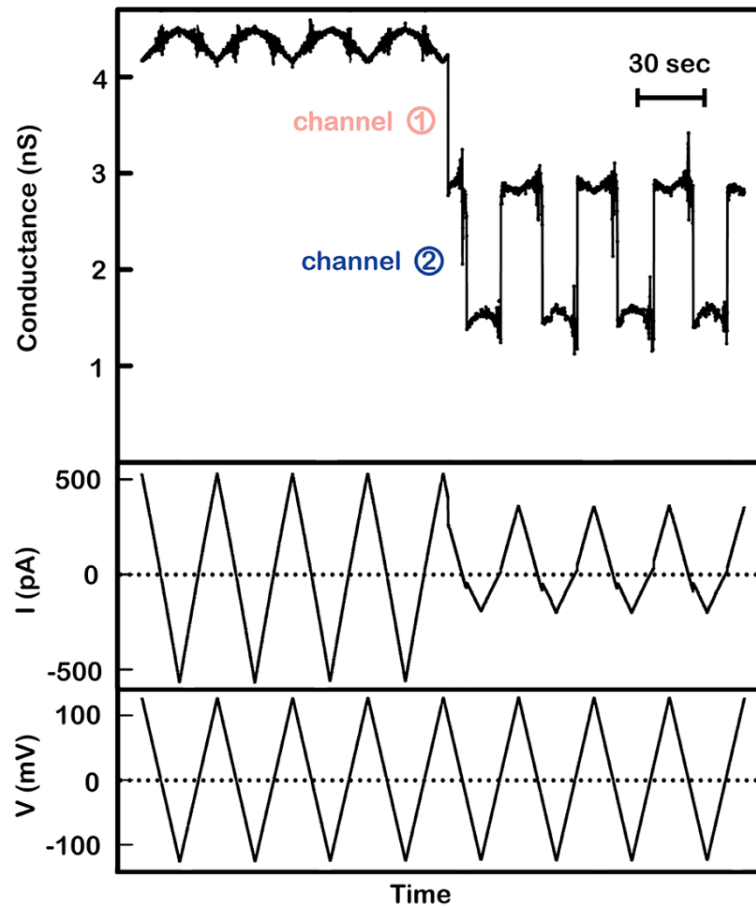
Fig. 4.5. Positive cooperativity between channel ① and ②. A single 4.4 nS conducting unit was probed using a 30 mHz (7.38 mV/sec) triangular voltage ramp (± 124 mV). From top to bottom, calculated conductance, current, and voltage traces are shown, respectively. Closure of channel ② at negative potentials only occurred after closure of channel ① at a high positive potential (here at 98 mV). Note that in the absence of gating the conductance varies somewhat with voltage due to a small amount of rectification in these channels. This is typical of 5 separate experiments.
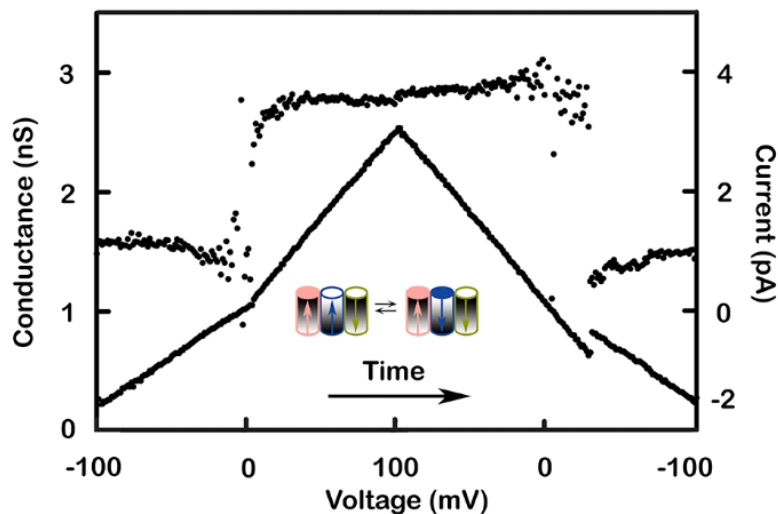
Fig. 4.6 Gating pattern of channel ②. The cartoon shows the closure and reopening as part of the model described in Fig. 4.12. The membrane contained a single Bax conducting unit and by the time this segment was recorded, channel ① had closed. Illustrated is the current recorded (lower trace) during one cycle of a triangular voltage wave (31 mHz, ± 100 mV). The upper trace is the calculated conductance. One can see that channel ② reopened at nearly zero, as the voltage became more positive, and closed at negative voltages.
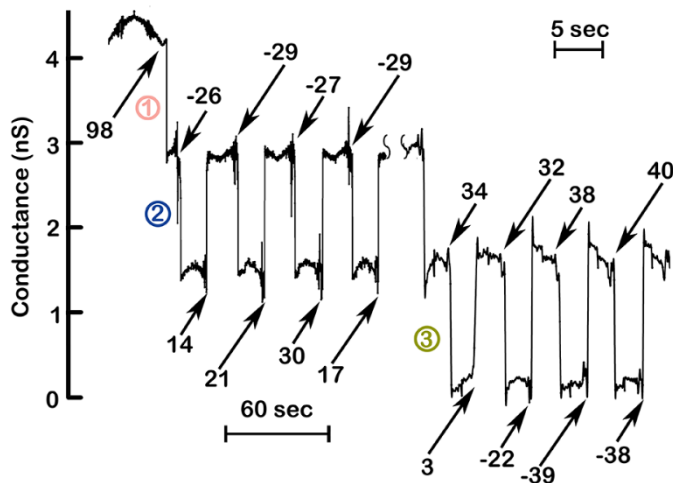
Fig. 4.7 Steep voltage dependence and cooperativity of channel ② and ③. The results illustrated in Fig. 4.5. were supplemented with data collected later in the same experiment recorded in the presence of higher frequency rate triangular ramps (175 mHz; 43.05 mV/sec). The numbers indicate the voltages at which the channels closed or opened. Channel ② closed at nearly identical voltages (-26, -29, -27, -29 mV), whereas reopening was delayed to positive voltages due to slower kinetics. At higher frequencies (right), these slow reopening kinetics resulted in channel ② remaining closed at the positive potentials needed to close channel ③.

63

(A)

(B)
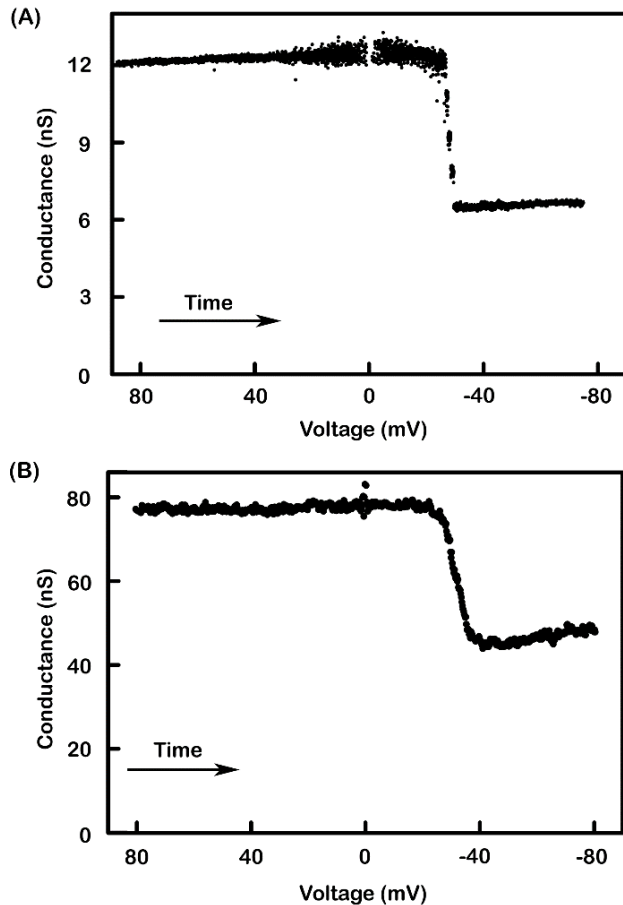
Fig. 4.8 Closure of channel ②'s in a membrane containing multiple Bax conducting units. (**A**) As voltage changed from positive to negative values, four channel ② closures (4 × 1.5 = 6 nS) were detected. The conductance dropped from 12.5 nS to about 6.5 nS. The residual conductance is that expected for 4 channel ③'s remaining open. All 4 units gated in this case. (**B**) The conductance decreased from 77 nS to 45 nS, equivalent to 21 channel ②'s closed (77 nS– 45 nS = 32 nS = 21 × 1.5 nS). In order for these 21 channel ②'s to close, 21 channel ①'s must have been closed. Therefore the original conductance should have been 77 nS + 21 × 1.5 nS = 109 nS; equivalent to 24 units (4.5 nS per unit). This is further confirmed by the final conductance after channel ② closure. The remaining conductance fits with 21 gating units (with only channel ③'s still open, 1.5 nS per unit) plus 3 non-gating units (4.5 nS per unit): 21 × 1.5 + 3 × 4.5 = 45 nS.

Within each of the 5 single-triplet experiments, the chance of observing a closure of channel ②, among all the ramps, was 92 ± 5 (5)% (total of 215 ramps at slow rates between 4.3 to 7.4 mV/sec). The closing of channel ③ took place only rarely with a slow voltage ramps but occurred more often at *higher* rates of change in voltage (Fig. 4.7, 4.9, 4.10). For example, the occurrence of the closure of channel ③ changes from 26 ± 18 % (in 215 ramps) to 84 ± 6 % (in 67 ramps) when the rate of voltage change was increased. Channel ③ closure occurred at positive potentials with the V_0 of 28 ± 2 (4) mV and reopening occurred as the positive potential declined (Fig. 4.11).
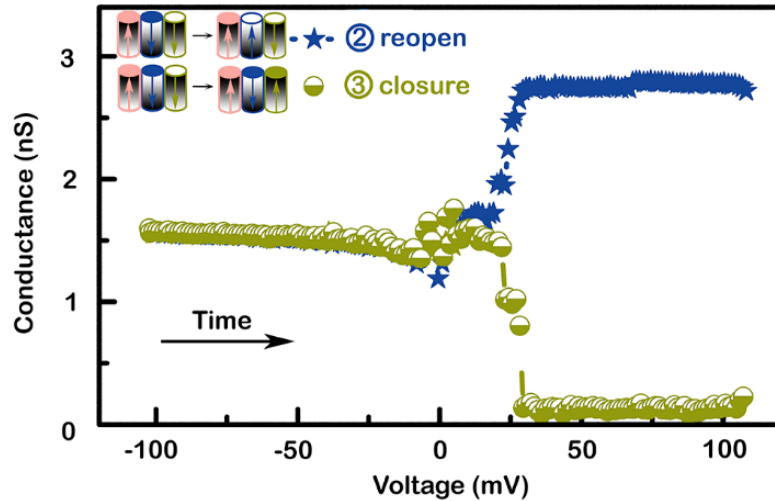
Fig. 4.9 Two possible gating modes when the voltage becomes more positive. The cartoons show how these two gating processes are explained by the model in Fig. 4.12. A single conducting unit was probed with a 31 mHz triangular voltage wave (± 101 mV). Starting with channel ② closed at high negative potentials, as the voltage reaches positive values it favors channel ② reopening and channel ③ closure but the cooperative behavior favors both channels to be in the same state. Experimentally two outcomes were observed: channel ② reopening (conductance increase to 3.0 nS) or channel ③ closure (conductance decrease to 0 nS). Thus the cooperativity dominated the outcome. This is typical of many experiments.
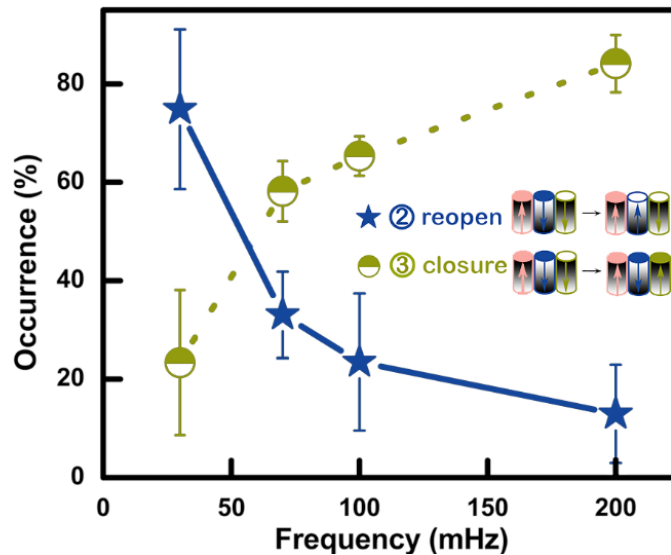
Fig. 4.10 Higher frequency triangular voltage waves favor the closure of channel ③, over the reopening of channel ②. The cartoons show how these two gating processes fit in the model described in Fig. 4.12. When channel ② was closed (G ~ 1.5 nS for single-unit experiments) and the voltage went toward positive values, the conductance either increased to 3 nS (indicating channel ② reopening) or decreased to 0 nS (indicating channel ③ closure) (see Fig. 4.9). By pooling many recordings from 5 separate single-triplet experiments, the relationship between the occurrence of these two events and the frequencies applied is shown here. As the frequency increased, channel ③ was more likely to close.

65
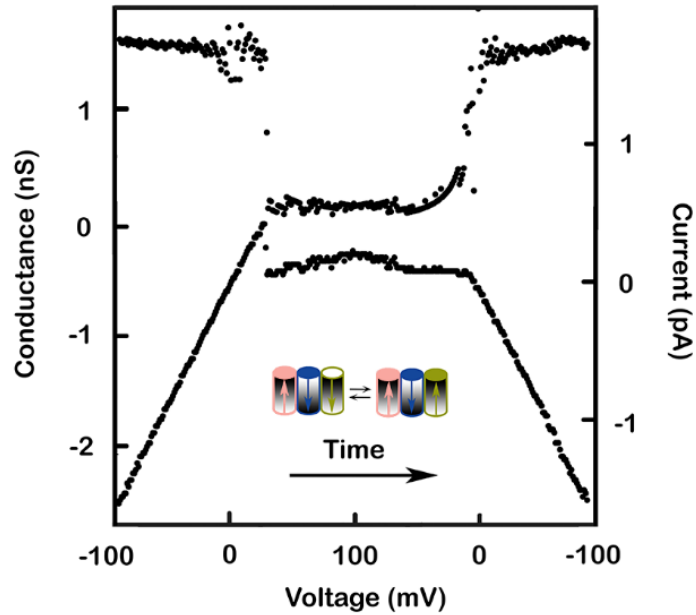
Fig. 4.11 Gating pattern of channel ③. The cartoon shows the closure and reopening as part of the model described in Fig. 4.12. The membrane contained a single Bax conducting unit and by the time this segment was recorded both channels ① and ② had closed. Illustrated is the current recorded (lower trace) during one cycle of a triangular voltage wave (31 mHz, ± 100 mV). The upper trace is the calculated conductance. Channel ③ closed at positive voltages. Note that the conductance only changed between 0 to 1.5 nS, indicating that channel ③ was the only channel that gated under these conditions. This was observed many times in each of 5 single triplet experiments.

These results and others presented below can be understood in the context of the model illustrated in Fig. 4.12. Although this is merely a model, its success in explaining rather complex behavior gives it some degree of solidity. Alternatives that we can conceive are far more complex and thus far less attractive. We propose that the fundamental conducting unit of 4.5 nS is a triplet of structurally identical channels in a linear organization (Fig. 4.12).

66
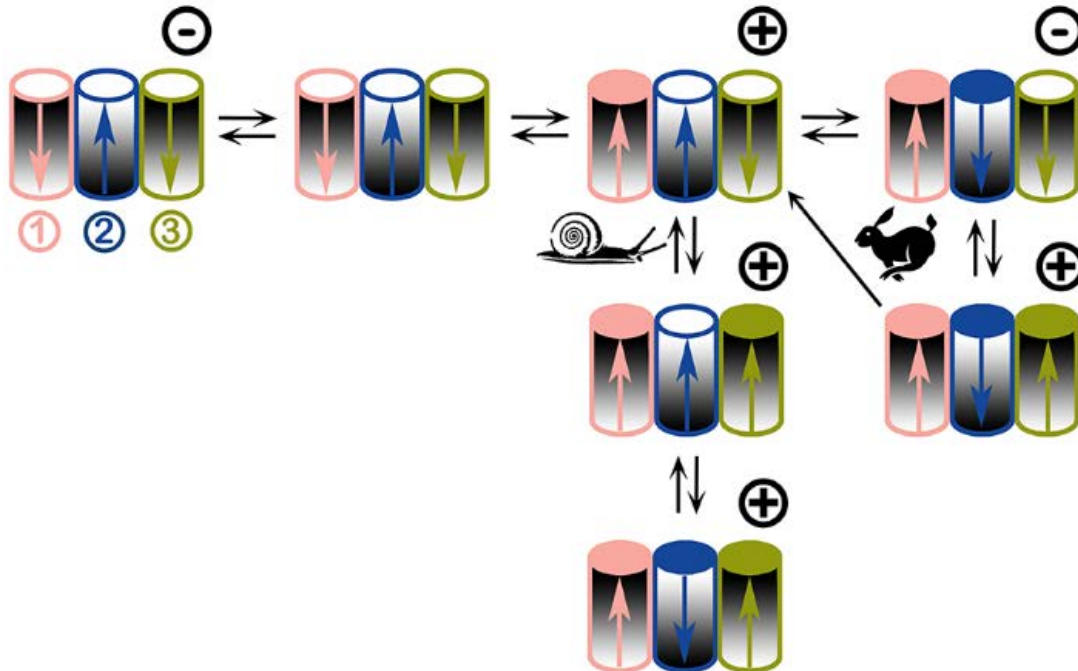
Fig. 4.12 Proposed voltage-gating model of Type A Bax channels. Each 4.5 nS conducting unit consists of three cylindrical channels arranged in a row. Each channel is likely formed by several Bax proteins. Here the light pink, blue, and olive green represent channel ①, ② and ③, respectively. The shading direction represents the orientation of the channels, with the middle cylinder (channel ②) having an opposite orientation compared to its neighbors. Arrows indicate the dipole moment of each channel, originating from the distribution of gating charge. The tip of the arrow is the negative end. Open circles at the end of a cylinder designate an open channel, solid circles, closed channels. Channel closure translocates the charged voltage sensor inverting the dipole moment, not the channel itself. Adjacent channels interact cooperatively, preferring to be in the same conformation: i.e. both open or both closed. This cooperativity may arise from dipole-dipole interactions between the voltage-sensor dipoles of each channel. The applied voltage is indicated by the sign at the upper right corner of each conducting unit. With no potential applied, all three channels are open (upper left). Applying a high positive voltage induces closure of channel ① whereas a negative voltage results in no closure. *Snail path*: at a constant voltage, channel closure is inhibited by the stabilizing effect of adjacent dipoles resulting in slow rates of closure. Yet a high positive voltage closes both channel ① and ③. Channel ② is forced to close through cooperativity with its neighbors, even though the sign of the voltage applied does not favor closure. *Rabbit path*: using triangular voltage ramps, the closure of channel ① favors closure of channel ② due to the dipole-dipole interaction. Channel ② closes at negative voltages. The cooperativity between ② and ③ requires ② to be closed for ③ to close. Fast triangular voltage ramps and the slow opening kinetics of channel ② result in ② remaining closed at positive potentials, allowing channel ③ to close (all-closed mode at the lower right). From there, as the voltage is reduced either channel ③ reopens followed by channel ② or channel ③ and ② can reopen simultaneously (one-way arrow).

A linear organization seems to best represent the functional behavior, since channel ① only affects the gating of channel ②, and closure/reopening of channel ③ is tightly related to the state of channel ②. From the sign of the voltage at which the

67

channels gate, it is proposed that channel ① & ③ are oriented in one direction and ②

is oriented in the opposite direction (shading direction indicates orientation). The

arrows in the individual channels describe the orientation of the voltage sensor as a

dipolar charge asymmetry and this direction inverts upon voltage-dependent channel

closure. Note that this is NOT the orientation of the channel itself, just the voltage

sensor domain. The orientation of the voltage sensor illustrated accounts for the sign of

the voltage gating as observed experimentally (Fig. 4.7). Each channel is most likely

an oligomer of Bax proteins [215] and the uniformity of the conductance decrements

following the application of a constant 70 mV potential [209] argues strongly for

structurally identical channels, each with the same number and organization of

monomers. The behavior described is best explained by a strong positive cooperativity

between the channels at the site of channel-channel interaction. The cooperativity

strongly favors the channels to be in the same conformational state, either all open or

all closed. The dipolar charge asymmetry of the voltage sensor could contribute or

perhaps be THE CAUSE of the strong cooperativity. Thus closure of the first channel

is unfavored (i.e. slow rate of closure even at high positive potentials probably due to

the positive cooperativity between ① and ②). When it occurs it requires a high positive

potential (Fig. 4.7) and is due to the closure of either channel ① or ③. As these are

identical in location and interaction, once one of these closes, that one is defined as

channel ①. Closure of channel ① not only removes the inhibition of closure on

channel ② (the dipole-dipole interaction) but actually favors the closure of ②. Thus

only a smaller potential is needed to close channel ② and the kinetics of this process

are fast (i.e., gating of channel ② by triangular voltage ramps takes place with remarkable regularity, Fig. 4.5 and rabbit symbol in Fig. 4.12). For channel ③ to close, it requires both a positive potential and a closed ② (the positive potential acting on the voltage sensor dipole and closure of channel ② removing the favorable dipole-dipole interaction). However, a positive potential also leads to channel ② reopening and thus ③ does not have the conditions for closure. By using a higher rate of voltage change one takes advantage of the relatively slow reopening kinetics of channel ② and thus achieve the conditions necessary for the closure of channel. Fig. 4.9 shows the two outcomes of rising voltages from negative to positive values, either channel ② reopens or channel ③ closes. At elevated positive potentials both must be open or both closed. From what we observed, the reopening of channel ② and ③ is highly dependent on the rate of voltage change, meaning that the reopening process is slow and thus kinetically delayed. The closing process is much faster and thus it was the closing process that was analyzed to determine the voltage-dependent parameters (Fig. 4.13). Note that the mid-point of the voltage range at which the gating occurred, V_0, of the closure process and that of the reopening process became the same as the rate of voltage change tended toward zero.

The slow kinetics of reopening is evident from the shift in the voltage at which channel ② reopens (Fig. 4.6, 4.13). At the higher rate of voltage change, the reopening of channel ② is delayed allowing one to achieve conditions suitable for ③ closure (Fig. 4.11). Once channel ③ closes, ② is inhibited from reopening due to the effects of cooperativity (Fig. 4.7) (note the favorable dipole-dipole interaction, Fig. 4.12). Indeed,

when channel ③ is closed, the reopening of ② occurs virtually simultaneously with the reopening of channel ③ (Fig. 4.14), demonstrating strong cooperativity. Indeed the two re-openings occurred simultaneously at the degree of temporal resolution used in the experiments: 2 to 5 msec depending on the experiment.
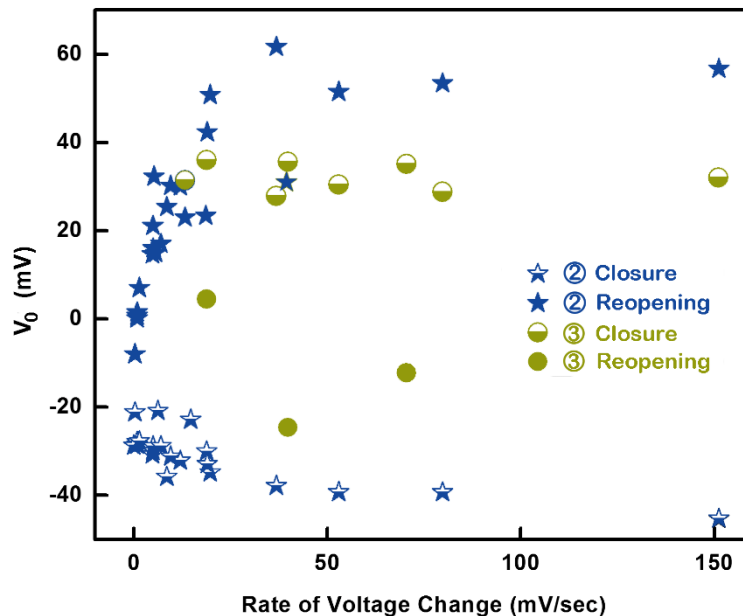
Fig. 4.13 The voltage range at which channel ② and ③ gating occurs depends on the rate of change of transmembrane voltage. V_0 from separate experiments was plotted against the rate of change of voltage used in the experiment. The parameter was determined either in the direction that led to channel closure or in the reopening direction. A total number of 11, 10, 2, 3 experiments were used here for channel ② reopening, channel ② closure, channel ③ reopening, channel ③ closure, respectively. Typically multiple rates were tested within each experiment.

The model also explains the staircase of closing events when a constant 70 mV potential is applied (Fig. 4.4). At constant high positive potential, the closure of channels ① and ③ is favored. When both of these are closed, the strong cooperative effect allows channel ② to close despite the wrong sign of the potential (Fig. 4.2). The conflicting actions of the electric field and the cooperativity result in a slow rate of closure indicated by the snail in Fig. 4.12.
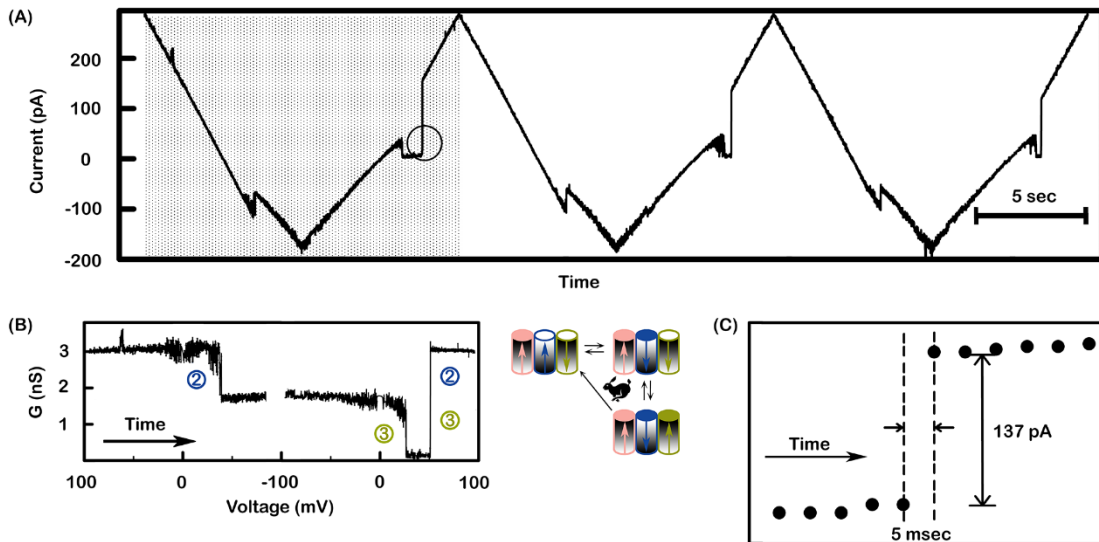
Fig. 4.14 Cooperative, virtually simultaneous reopening of channel ② and ③. A single 4.5 nS conducting unit was probed with a 71 mHz (13.63 mV/sec) triangular voltage ramp. (**A**) The current recorded for 3 successive voltage ramps showing essentially simultaneous reopening of channels ② and ③. (**B**) Conductance vs. voltage plot of the data in the dotted area in (*A*). Both (*A*) and (*B*) show channel ② closure at a negative voltage, then channel ③ closing as the potential became positive, followed by simultaneous reopening of channels ② and ③. (*C*) Expanded view of the circled area in (*A*) showing that the current increased within 5 ms. This was observed in all 7, single triplet experiments.

Further evidence of the model comes from its ability to account for conductance changes observed with multi-unit experiments. In Fig. 4.15*A*, only 4 closures of channel ② were observed. This indicates that 4 channel ①'s ($1.5 \times 4 = 6$ nS) must have been closed beforehand to allow these channel ②'s to close. Therefore, the all-open conductance should be $21 + 6 = 27$ nS, equivalent of 6 conducting units. The remaining conductance after the 4 channel ② closures is consistent with 4 open channel ③'s (4×1.5 nS) plus 2 triplets (2×4.5 nS) that were not gating resulting in as total conductance of 15 nS. This interpretation is further illustrated in an experiment with many triplet units (Fig. 4.15*B*).

71
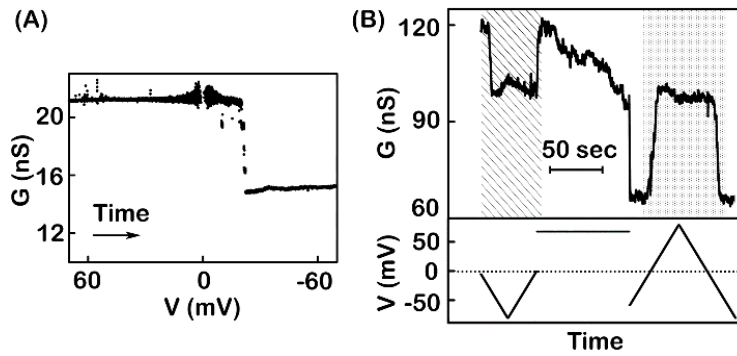
Fig. 4.15 Supportive evidence of the model: multi-unit examples. (**A**) A 2 mHz (0.28 mV/sec) triangular voltage (± 70 mV) ramp was applied to a membrane containing multiple conducting units. The voltage changed from positive to negative values and at -20 mV, 4 decrements occurred, indicating the closure of 4 channel ②'s. The remaining conductance (15 nS) is consistent with the 2 non-gating units and the 4 gating units with only channel ③'s open. Therefore at positive voltages the conductance was composed of 2 non-gating units and 4 units with their channel ① closed (3.0 nS per unit) for a total of 21 nS. (**B**) A 9 mHz (1.44 mV/sec) triangular voltage ramp (± 80 mV) was applied to the membrane resulting in conductance changes at negative potentials of 17 nS, equivalent to the closure and reopening of 11 channel ②'s (each 1.5 nS) (striped area). Thus only 11 units had a closed channel ①. The subsequent application of 70 mV for 85 s resulted in a conductance decrement of 24 nS, equivalent to the closure of 16 channel ①'s. Reapplication of the triangular voltage ramp (dotted area) showed conductance changes at negative potentials of 38 nS, equivalent to the closure and reopening of 25 channel ②'s.

Following the same logic, the total conductance on the left panel is consistent with about 19 non-gating triplets (all channels open) and 11 gating triplets (determined from channel ② closures). A 70 mV potential was applied for 82 s resulting in the equivalent of *16*, 1.5 nS conductance decrements, presumably from more channel ①'s being closed. The reapplication of a triangular voltage ramp resulted in 38 nS worth of channel ② gating, consistent with *14* more gating triplets. Again the model explains the observed conductance changes. Finally, we used a voltage pulse sequence that allowed rapid closure of channel ② and ③ by applying a negative potential followed by a positive potential (Fig. 4.16). In illustrated experiment, a negative potential caused immediate closure of two channel ②'s followed by a step to a positive potential

72

resulting in immediate closure of two channel ③'s. Paired reopening of ② & ③ in

two double-channel steps resulted in return to the initial conductance.
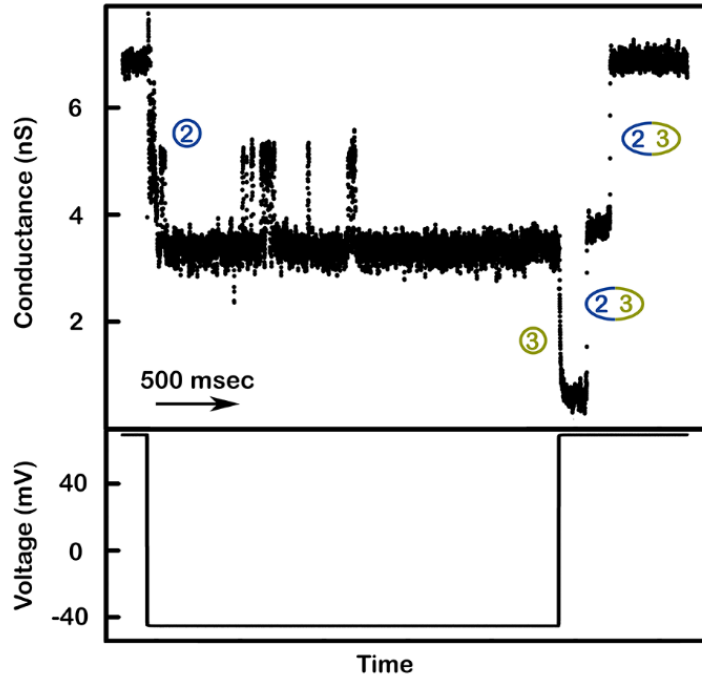
Fig. 4.16 Model tested by voltage pulse sequence. This membrane contained two conducting units. First the voltage was stepped from +69 to -45 mV in order to close the two channel ②'s. A rapid drop in conductance (<47 msec) of ~3.4 nS was observed, consistent with about two channel ②'s closures. Then the voltage was stepped back to 69 mV to close channel ③ before channel ② could reopen. An immediate decrement of conductance from 3.3 to 0.5 nS was seen, indicating the closure of two channel ③'s. Soon after the drop, two increments, each with about 3 nS, were detected. This was interpreted to be the synchronized reopening of two sets of channel ③ and channel ②. This recording is typical of many observations.

The rapid kinetics of channel ② closure allowed us to assume the achievement

of a quasi-equilibrium between the open and closed state during the voltage change

resulting from the applied triangular voltage ramp. Therefore a measure of the effective

gating charge, n, was obtained by fitting to the Boltzmann distribution (Fig. 4.1). These

values depended on the rate of change in voltage indicating that the kinetics of the

process was still limiting. Thus the values of n were plotted against the rate of voltage

73

change and its value at zero rate was determined by extrapolation. The resulting n of

14 ± 2 rivals those of the voltage-gated channels responsible for the electrical

excitability of neurons and muscles (Fig. 4.17).
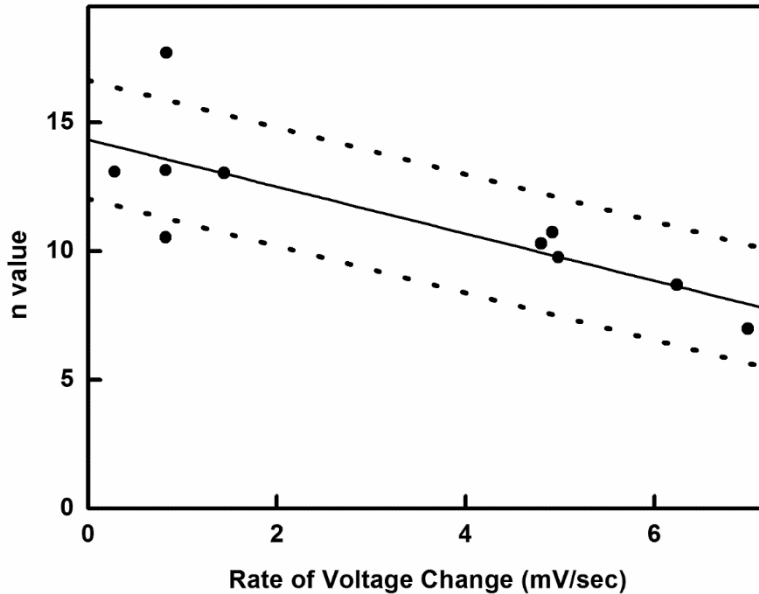
Fig. 4.17 Estimate of the effective gating charge, n. This is a quantitation of the gating of channel ② (see Fig. 4.1 and Methods for details). Points represent the n values calculated for experiments performed at the indicated rate of voltage change. The data was pooled from nine separate experiments. The solid line is the least squares fit and the dotted lines show the 95% confidence limits. The extrapolated n value at zero rate (equilibrium value) is 14 ± 2.5.

4.5 Discussion

The electrophysiological properties of Bax channels strongly support the

conclusion that these are organized in a triplet structure in which the channels exhibit

a high degree of positive cooperativity and steep voltage dependence. The channels

prefer to be in the same state whether it be the closed or open state. Further, this

cooperativity seems to be limited to pairs of likely adjacent channels: ①/② and ②/③

. The voltage-dependent closure of channel ① & ③ at positive potentials and

channel ② at negative potentials is most simply explained by channel ② being oriented

in an opposite direction to ① & ③. This opposite orientation could account for the cooperativity if it were based on a charge dipole of the voltage sensor. An opposite orientation of adjacent channels would result in a favorable dipole-dipole interaction (①/② and ②/③) (Fig. 4.12). The movement across the membrane of the voltage sensor upon channel closure would invert the dipole (invert the direction of arrows in Fig. 4.12) resulting in electrostatic repulsion rather than attraction between adjacent channels and thus favor closure of the adjacent one. This model works best if the triplet is organized as a linear arrangement of channels, with channel ② in between ① & ③. Thus channel ① and ③ are essentially identical but their behavior differs once one of these closes. The steepness of the voltage dependence and thus the requisite movement of a large amount of gating charge from one side of the membrane to the other in opposite directions cannot be easily explained by anything other than an opposite orientation for these channels, despite the obvious concerns on how that could take place. Typically the channel's structure, such as a large surface domain (e.g. α-hemolysin [216]), limits insertion in only one direction. However VDAC channels have been shown to be able to insert into planar membranes in both directions [188,217]. In addition, colicins, toxin channels that have been reported to have similarities to Bcl-2 family proteins, translocate most of their mass to the opposite membrane surface when they insert into a phospholipid membrane [218]. Thus there is no serious theoretical impediment to the possibility of Bax channels inserting in opposite directions save those arising from the need to be skeptical with regard to any novel proposal.

A Boltzmann distribution analysis of the voltage dependent conductance of channel ② yielded an estimate of the effective gating charge. The value of 14 that was

obtained is twice that reported for the voltage gated channels responsible for electrical excitability in animal cells when channel activation was analyzed by similar methods [72,219]. When charge was estimated by measuring displacement currents [219,220] then values comparable to those reported here were obtained. Thus the steepness of voltage gating we observed is extremely high indicating an as yet undefined but important role in the physiological function of Bax. The closure instead of the reopening process was used for analyzing both channel ② and ③ gating here, due to the substantial kinetic delay of the reopening process (Fig. 4.13). The delay makes one unable to study the gating of the channel with the assumption that it's very close to equilibrium. Therefore, the one with less delay, the closure, was used here. The calculated parameters that define the gating process, n and V_0, should be the same regardless of which process is analyzed, the reopening or the closing process. However, we found that, although the V_0 of closure and reopening extrapolate to the same value at zero rate of voltage change, the n values don't seem to do this (Fig. 4.18). It may due to our inability to measure these values at low enough rates combined with a non-linear rate dependence of this value. It is also possible that the gating process exhibits true hysteresis. An explanation may emerge as more information about the gating mechanism is uncovered.

The very steep voltage dependence requires a highly charged voltage sensor domain and that can be reconciled with the protein structure if each channel is an oligomer of numerous Bax proteins. The oligomeric nature of the Bax channel is well accepted in the literature and there are various insights into how this oligomerization might take place [174–176,221,222]. Furthermore, studies have provided compelling evidence that helices 5, 6 and 9 are inserted into the membrane [195,196]. The high positive charge

76

of helix 5 makes this helix an attractive candidate for the voltage sensor. Positively

charged helices have been shown to be the voltage sensors in the $Na^+/K^+/Ca^{2+}$ family

of voltage-gated channels [223].

Figure 4.18 The effective gating charge, n, varies with the rate of change of the applied voltage for both the closure and reopening processes. The n values were calculated using the Boltzmann distribution from data collected for the reopening (solid circles, N=11) and closure (open circles, N=10) of channel (2). More than one rate of voltage change was often recorded within each experiment.

The structure of Bax in the mitochondrial outer membrane and the properties of

Bax channels have been studied extensively, but the overall level of understanding is

quite limited. For example, the number of monomers per functional channel is still not

clear. This number varies from four [197] to greater than a hundred [198]. Similar studies of

the MAC channel [184] are consistent with channels of varying size.   The published

properties of conductance formed by the Bax protein also vary in magnitude. Some of

this variation may arise from a heterogeneity of channel sizes and some from the source

or treatment of the protein. Certainly the Type B channels formed by Bax vary in size

probably because they can grow to any size. None of the published conductance clearly correspond to the properties of the Type A channels reported here. The reasons for these differences may have to do with methods of protein isolation and handling. Also the MAC channel being obtained from mitochondria undergoing apoptosis, is likely to be a far more complex structure that one formed from pure Bax protein.

The physiologically relevant role of the characteristics presented here is not clear yet. Obviously voltage gating of Bax channels requires a controllable potential across the mitochondrial outer membrane (MOM). Although somewhat controversial, the potential across the MOM was measured to be about -30-40 mV [200,202], and calculated to be able to reach a magnitude of ~60 mV [201]. The potential would be very sensitive to the dynamic flux of charged metabolites [201] and the charge of macromolecules in the cytosol and intermembrane space [200]. These change during the apoptotic process and thus could influence the conformational state of Bax channels. Another voltage gated channel exists in the MOM: the VDAC channel. VDAC is found in all eukaryotic kingdoms and responsible for metabolite flux across the MOM. The canonical isoform has remarkably conserved voltage gating parameters [153,224] indicating strong evolutionary selection. Yet, voltage gating can easily be altered by single point mutations without affecting channel formation or metabolite flux [225]. Thus, the voltage-gating properties are conserved to allow VDAC to be controlled by the potential across the MOM. Similarly, the properties of Bax may have evolved to respond to the same potential.

4.6 Acknowledgements

CHAPTER 5: **DISCUSSION AND FUTURE DIRECTIONS**

5.1 Gating Model

The bacterial protein reported here can form cation-selective channels with a diameter about 0.9 nm, steeply voltage-gated, and high degree of cooperativity. When triangular voltage ramps were applied, they showed steep voltage dependence (gating charge n~14) and remarkable cooperativity between channels. A model was proposed based on these features: the conducting unit is composed of three identical channels, in a linear fashion, with the center one (channel ②) having the opposite orientation. The voltage sensor domain is modeled as a dipole, one per channel, and the dipole-dipole interactions between these three channels arising from the opposite orientation of the centric channel ② stabilize the structure. A similar scenario would exist if the voltage sensor were a charged group. The strong cooperativity is apparent when channel ② and ③ reopen together at low positive voltages. Additionally, these three channels prefer all-closed or all-open conformations, due to the dipole-dipole interaction. Because of the unique and unprecedented gating behaviors, the physiological functions behind the channel reported here must be a result of strong evolutionary pressure.

5.2 Comparison to Known Channels

5.2.1 Comparison to Known porins

Because of the large single channel conductance, the triplet behavior, the fact that the channel activity still existed after dialysis, and that the channel former is from E. coli, it's possible that the channel discussed here is closely related to porins. Despite

the above similarities, compared to other voltage-gated porins, several differences still exist. (1) The n value (the number of charges moving across the field upon gating) is much larger than that of porins. (2) The gating voltage (V_0) is lower than that of porins, whose V_0 are generally above 100 mV. (3) The cooperativity among channels is strong and unprecedented. (4) Two types of channel activity were observed (Type A and Type B). OmpA is the only other porin found to form two distinctly different types of channels. The majority of the OmpA channels observed have an extremely low conductance whereas some form channels with a much larger conductance [226]. However, none of these two conformers of OmpA show voltage gating.

Nevertheless, other parameters such as the pore diameter and the selectivity of the channels studied here are similar to those of OmpF. The diameter of the channels presented here is about 0.9 nm, calculated from the single channel conductance. The constriction zone of OmpF is about 7 x 11 Å [66], which is big enough for most antibiotics, ions, etc. to pass through. This indicates possible roles for the channel reported here as a pathway for molecules to cross the outer membrane. Moreover, the selectivity of the channel of interest (P_C/P_A = 3.6 ± 0.3, see section 3.4.4) is similar to those of OmpF and LamB (see Table 1.2).

5.2.2 Comparison to Known Voltage-Gated Channels

Compared to other voltage-gated channels, the n value of the channel reported here (n = 14) is much larger, even greater than that of voltage-gated potassium channels (n = 4) (Table 5.1). The measured gating charge of voltage-gated potassium channels is about 14, which is comparable to the channels shown here. Note that the gating charge is the actual number of charges involved in the gating process. If the coupling

between the VSD and pore domain is weak, the n value would be lower than the gating charge. Generally the gating charge is either equal or larger than the n value. The V_0 for the channel reported here is much lower than that of some porins (e.g. OmpF, OmpC), and it is in a reasonable range of the Donnan potential present under normal environmental conditions (not very dilute solutions).

The voltage-gated potassium/sodium/calcium channel family is highly conserved, and these channels play a key role in the formation and propagation of the action potential. For the channel described in this dissertation, since the n value is much higher than that of the voltage-gated potassium channel, important roles from natural selection are indicated here.

Table 5.1 Properties of some voltage-gated channels

	Open channel conductance (1M KCl)	Selectivity (P_c/P_a, 0.1M/1M KCl)	Pore size (nm)	n value (gating charge)	V_0 (mV)	# of monomers
K$^+$ channels	3.7 pS ρ [147]	-	0.4 [148]	4(14) [149–151]	-58 (fast) or 7 (slow) [152]	4
VDAC	4.5 nS [153]	0.59 [154]	2.5 [107]	2 [155], 4.9 ± 0.5 or 3.6 ± 0.2 [156]	-28 ± 4, 5.2 ± 0.4 [156]	1
OmpF	0.84 ± 0.06 nS [157]	3.5 ± 0.5 [158]	0.7 [66]	-	145 ± 7 [157]	3
	1.5 ± 0.04 nS	3.6 ± 0.3	0.9	14 ± 2.5	-27 ± 4, 28 ± 2	-

ρ: 140 mM KCl
ϕ: Depending on the experimental conditions.

84

5.3 Possible Physiological Function Of These Voltage-Gated Channels

Due to the existence of nonspecific porins in the outer membrane, it is generally impossible to have any transmembrane potential across the outer membrane, except the Donnan potential. The Donnan potential arises from the polyanionic oligosaccharide in the periplasmic space. However, the measured Donnan potential was less than 30 mV (with 100 mM of cation concentration in the bulk solution) [132,227]. The transmembrane potential across the inner membrane, on the contrary, is much larger: it's around -100 mV to -140 mV, depending on the environment [228]. Although the channel ② reported here can be closed at low voltages (-27 ± 4 mV, see section 4.4), it requires much higher potential to close channel ①. It's not clear where the channels should be located so that the existing membrane potential fits with the voltage gating properties of this novel channel.

Despite that, because of the steep voltage dependence and the physiologically relevant V_0 (for channel ② and ③), it is possible that the channel reported here plays an important role in the regulation of the permeation of small metabolites, nutrients, and antibiotics. Antibiotics resistance has been an increasingly serious issue. Compared to the modification of the antibiotic target or expression of enzymes, changing the permeability of the outer membrane is effective for a wider spectrum of antibiotics for the bacteria.

Porins are known to be involved in the diffusion of many antibiotics across the outer membrane [229,230]. For bacteria, multiple strategies have been used to survive the environment with antibiotics. Examples include decreasing the expression level of certain porins [231,232], expressing mutated porins with restricted permeability [233,234],

increasing the expression level of some efflux pumps [235,236], etc. For all the experiments presented here, ampicillin was added as a selection marker of pTYB1-Bax construct. pTYB1 carries a β-lactamase gene that digests ampicillin. Comparing the proteomes of different fractions of the cells, grown with or without ampicillin; and testing the samples from cells grown with or without ampicillin, may shed some light on the identity or function of the channel-forming proteins.

5.4 Identification of the channel former

Although the identity of this functional protein is not known yet, it is believed to come from the E. coli strain BL21(DE3)pLysS that was used to purify Bax. From the silver-stained SDS-PAGE results shown in Fig. 5.1, one can see that over 95 % of the contents is Bax. Considering the sensitivity of silver stain (0.25 ng, from Pierce Silver Stain Kit manual), this functional protein is a minor constituent of the purified fraction. Note that the purified sample was dialyzed against 3 L and then 5 L of buffer for total of 48 hours, with the cutoff size of the dialysis bag being 6000-8000 kDa. Therefore, it is more likely that the functional channel former is a protein, instead of small molecules (e.g. peptides, lipids, chemicals). First, it's important to determine in which cellular compartment the channel might reside. That should help reduce the number of potential candidates. Due to the fact that each conducting unit has three channels, this unknown channel may be related to the bacterial porins. If so then it should be located in the outer membrane. The relatively high single-channel conductance also resembles the porins. Clearly, having channels in the inner membrane can dissipate the transmembrane potential for the bacteria and thus this location seems less likely. A search for proteins whose sequence has homology to

porins may be prove useful. E. coli strains with specific porin(s) knocked out could allow the identification of the channel-former. If appropriate fractions from a knock-out strain fail to show the desired channel activity then it may be the right knock-out. Overexpression of that specific protein would be the next step to confirm the identity.

5.4.1 Identification of the Cellular Localization

The cell culture of E. coli can be separated into the following parts: the culture medium (the bulk environment for E. coli), the outer membrane, the inner membrane and the cytosol. Although all the tests reported in the previous chapters were done with the sample purified from the soluble fraction (i.e. the cytosol), it is possible that the channel reported here actually comes from other fractions. The channel former could be in the culture medium, being an exotoxin secreted from E. coli into the environment. The membrane fractions might also be the source. After all, it's rare for a channel-forming protein to be soluble to start with, such as Bax [174]. The culture medium can be tested by collecting the supernatant after spinning down the cell pellet. The membrane

Fig. 5.1 SDS-PAGE analysis of the purified Bax. The sample was purified following the method described in Section 2.2.2. About 450 ng of protein was added to the left lane, and about 225 ng of protein was added to the right lane.

fractions can be collected by the following method [237]. Generally, after obtaining the

membrane fraction, 2% n-laurylsarcosine (w/v) is used to solubilize the inner

membrane. The pellet obtained after this step contains the outer membrane fraction.

This can be solubilized with octyl-glucoside [238].

5.4.2 Comparison with Known Porins

Although many bacterial porins already have well-established properties [239,240],

experimental conditions such as of the lipid composition, the technique used to form

membranes, etc. may alter the results [158]. Therefore, a good starting point to find the

protein of interest would be to test the known porins, such as OmpC, OmpF, LamB,

etc.

5.4.3 Single/Multi-Porin Knock-Outs

E. coli strains such as Omp9 [BL21(DE3) Δ*lamB ompF*::Tn5 Δ*ompA* Δ*ompC*

ompN::Ω] [237] can be used to facilitate the above approach. Isolating the desired cellular

fraction from this strain and then testing it on the planar membrane can help to narrow

down the options. Furthermore, we may perform the protein BLAST search, with

known porins (e.g. OmpN, ScrY, OmpF) as query sequences. The SWISS-MODEL

(via ExPASY) can then be used to further estimate the tertiary structure of the

candidates from the BLAST search. Through this process, the open reading frames

that yield proteins showing channel structures are likely candidates. The corresponding

knock-out E. coli strains can be purchased from the Coli Genetic Stock Center. The

same protocol used to study Omp9 can be used to test other knock-out strains.

APPENDIX

The discovery that Bax was not responsible for the channel-forming activity described in this thesis, took place when samples were isolated as described in the methods but the E. coli that was used did not contain the plasmid, pTYB1-Bax. The E. coli strain used was BL21(DE3)pLysS, the same as the one that had previously been transfected with the plasmid. In the accompanying figure, panel A illustrates some of the results from an experiment done with the isolated sample lacking the plasmid. The rate of voltage change is 5.38 mV/sec. Panel B shows a plot of the averaged conductance against the applied voltages from the same experiment. The conductance was averaged from twenty waves showing the same gating pattern. The resulting n value from panel B is 9.9, and the V0 is -35.5 mV. At least five other experiments done with the sample isolated without pTYB1-Bax showed similar results. These results demonstrate conclusively that the channel former is not Bax.

(A)

(B)
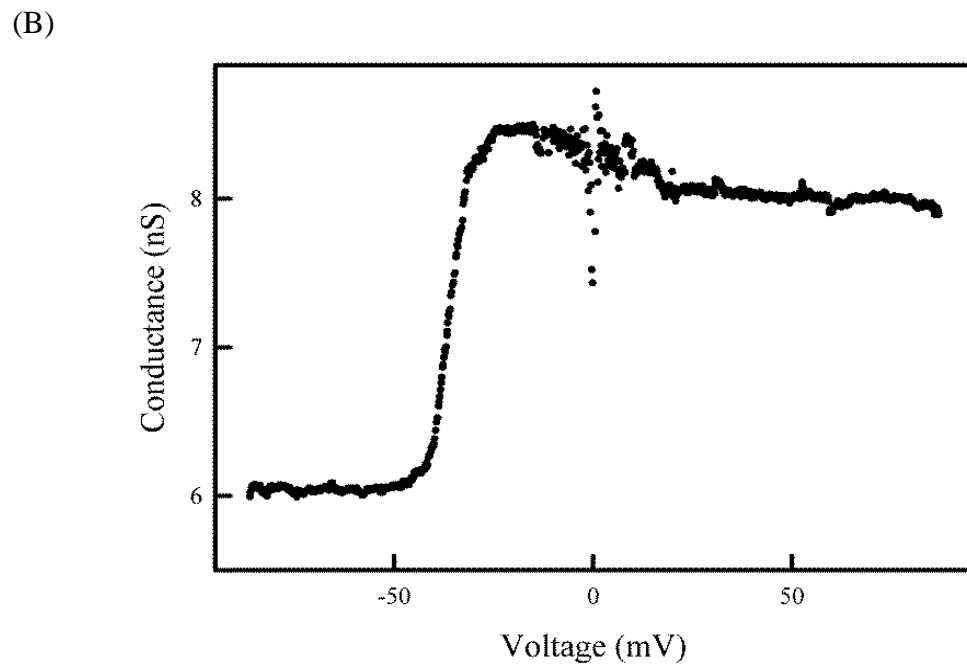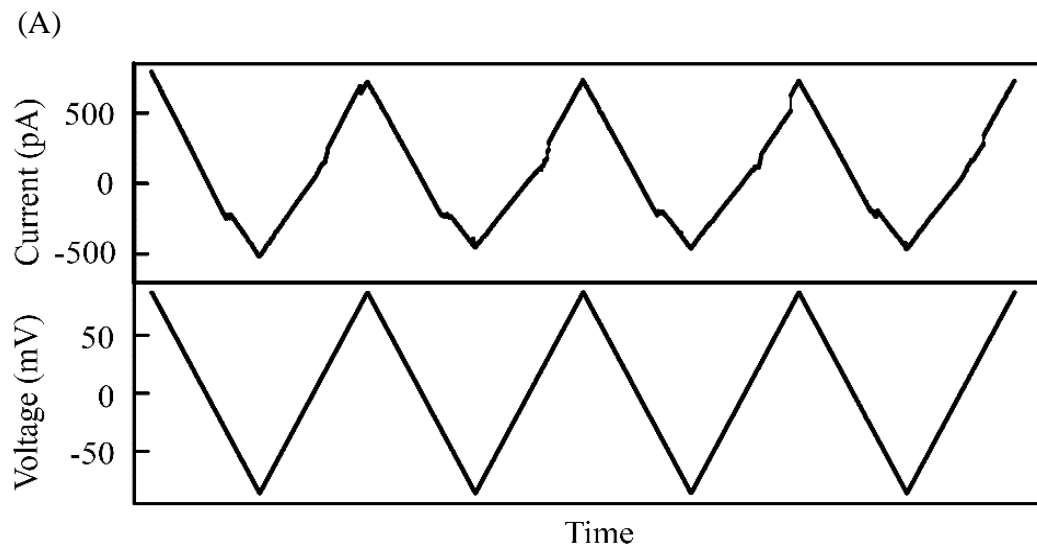
BIBLIOGRAPHY

1. Kornak, U. *et al.* Loss of the CIC-7 chloride channel leads to osteopetrosis in mice and man. *Cell* **104,** 205–215 (2001).

2. Stutts, M. J. *et al.* CFTR as a cAMP-dependent regulator of sodium channels. *Science* **269,** 847–850 (1995).

3. D'Adamo, M. C. *et al.* Novel phenotype associated with a mutation in the KCNA1(Kv1.1) gene. *Front. Physiol.* **5,** 1–10 (2015).

4. Sternberg, D. *et al.* Hypokalaemic periodic paralysis type 2 caused by mutations at codon 672 in the muscle sodium channel gene SCN4A. *Brain* **124,** 1091–1099 (2001).

5. Menestrina, G., Schiavo, G. & Montecucco, C. Molecular mechanisms of action of bacterial protein toxins. *Mol. Aspects Med.* **15,** 79–193 (1994).

6. Gonzalez, M. R., Bischofberger, M., Pernot, L., Van Der Goot, F. G. & Frêche, B. Bacterial pore-forming toxins: The (w)hole story? *Cell. Mol. Life Sci.* **65,** 493–507 (2008).

7. Coote, J. G. Structural and functional relationships among the RTX toxin determinants of gram-negative bacteria. *FEMS Microbiol. Rev.* **8,** 137–161 (1992).

8. *Pore-forming peptides and protein toxins*. **5,** (Taylor & Francis, 2003).

9. Maier, E., Reinhard, N., Benz, R. & Frey, J. Channel-forming activity and channel size of the RTX toxins ApxI, ApxII, and ApxIII of Actinobacillus pleuropneumoniae. *Infect. Immun.* **64,** 4415–4423 (1996).

10. Benz, R., Schmid, A., Wagner, W. & Goebel, W. Pore formation by the Escherichia coli Hemolysin: Evidence for an Association-Dissociation Equilibrium of the Pore-Forming Aggregates. *Infect. Immun.* **57,** 887–895 (1989).

11. Benz, R., Hardie, K. R. & Hughes, C. Pore formation in artificial membranes by the secreted hemolysins of Proteus vulgaris and Morganella morganii. *Eur. J. Biochem.* **220,** 339–347 (1994).

12. Bamberg, E. & Lauger, P. Channel formation kinetics of gramicidin A in lipid bilayer membranes. *J Membr Biol* **11,** 177–194 (1973).

13. Benz, R., Maier, E., Ladant, D., Ullmann, A. & Sebo, P. Adenylate cyclase toxin (CyaA) of Bordetella pertussis. Evidence for the formation of small ion-

permeable channels and comparison with HlyA of Escherichia coli. *J. Biol. Chem.* **269,** 27231–27239 (1994).

14. Ehrmann, I., Gray, M., Gordon, V., Gray, L. & Hewlett, E. Hemolytic activity of adenylate cyclase toxin from Brodetella pertussis. *FEBS Letters* **278,** 79–83 (1991).

15. Vojtova-Vodolanova, J. *et al.* Oligomerization is involved in pore formation by Bordetella adenylate cyclase toxin. *FASEB J.* **23,** 2831–2843 (2009).

16. Raymond, L., Slatin, S. L. & Finkelstein, A. Channels formed by colicin E1 in planar lipid bilayers are large and exhibit pH-dependent ion selectivity. *J. Membr. Biol.* **84,** 173–181 (1985).

17. Slatin, S. L., Raymond, L. & Finkelstein, A. Gating of a voltage-dependent channel (colicin E1) in planar lipid bilayers: the role of protein translocation. *J. Membr. Biol.* **92,** 247–254 (1986).

18. Hladky, S. B. & Haydon, D. A. Ion transfer across lipid membranes in the presence of gramicidin A. I. Studies of the unit conductance channel. *Biochim. Biophys. Acta* **274,** 294–312 (1972).

19. Myers, V. B. & Haydon, D. A. Ion transfer across lipid membranes in the presence of gramicidin A. II. The ion selectivity. *Biochim. Biophys. Acta* **274,** 313–322 (1972).

20. Pawlak, M., Stankowski, S. & Schwarz, G. Melittin induced voltage-dependent conductance in DOPC lipid bilayers. *Biochim. Biophys. Acta* **1062,** 94–102 (1991).

21. Rex, S. Pore formation induced by the peptide melittin in different lipid vesicle membranes. *Biophys. Chem.* **58,** 75–85 (1996).

22. Tosteson, M. T. & Tosteson, D. C. The sting. Melittin forms channels in lipid bilayers. *Biophys. J.* **36,** 109–116 (1981).

23. Mirzabekov, T. *et al.* Channel formation in planar lipid bilayers by a neurotoxic fragment of the beta-amyloid peptide. *Biochem. Biophys. Res. Commun.* **202,** 1142–1148 (1994).

24. Prangkio, P., Yusko, E. C., Sept, D., Yang, J. & Mayer, M. Multivariate Analyses of Amyloid-Beta Oligomer Populations Indicate a Connection between Pore Formation and Cytotoxicity. *PLoS One* **7,** (2012).

25.   Ardail, D. *et al.* Diversity and Complexity of Ceramide Generation After Exposure of Jurkat Leukemia Cells to Irradiation. *Int. J. Radiat. Oncol. Biol. Phys.* **73,** 1211–1218 (2009).

26.   Dai, Q. *et al.* Mitochondrial ceramide increases in UV-irradiated HeLa cells and is mainly derived from hydrolysis of sphingomyelin. *Oncogene* **23,** 3650–3658 (2004).

27.   Siskind, L. J., Kolesnick, R. N. & Colombini, M. Ceramide forms channels in mitochondrial outer membranes at physiologically relevant concentrations. *Mitochondrion* **6,** 118–125 (2006).

28.   Siskind, L. J., Davoody, A., Lewin, N., Marshall, S. & Colombini, M. Enlargement and contracture of C2-ceramide channels. *Biophys. J.* **85,** 1560–75 (2003).

29.   Siskind, L. J. & Colombini, M. The lipids C2- and C16-ceramide form large stable channels: Implications for apoptosis. *J. Biol. Chem.* **275,** 38640–38644 (2000).

30.   Samanta, S., Stiban, J., Maugel, T. K. & Colombini, M. Visualization of ceramide channels by transmission electron microscopy. *Biochim. Biophys. Acta* **1808,** 1196–201 (2011).

31.   Ganesan, V. *et al.* Ceramide and activated Bax act synergistically to permeabilize the mitochondrial outer membrane. *Apoptosis* **15,** 553–62 (2010).

32.   Siskind, L. J. *et al.* Anti-apoptotic Bcl-2 Family Proteins Disassemble Ceramide Channels. *J. Biol. Chem.* **283,** 6622–30 (2008).

33.   Martinac, B. The ion channels to cytoskeleton connection as potential mechanism of mechanosensitivity. *Biochim. Biophys. Acta - Biomembr.* **1838,** 682–691 (2014).

34.   Sukharev, S. I., Blount, P., Martinac, B. & Kung, C. Mechanosensitive channels of Escherichia coli: the MscL gene, protein, and activities. *Annu. Rev. Physiol.* **59,** 633–657 (1997).

35.   Blattner, F. R. *et al.* The complete genome sequence of Escherichia coli K-12. *Science* **277,** 1453–1462 (1997).

36.   Meier-Kolthoff, J. P. *et al.* Complete genome sequence of DSM 30083T, the type strain (U5/41T) of Escherichia coli, and a proposal for delineating subspecies in microbial taxonomy. *Stand Genomic Sci* **9,** (2014).

37. Lee, S. Y. High cell density culture of Escherichia coli. *Trends Biotechnol.* **14,** 98–105 (1996).

38. Russo, E. The birth of biotechnology. *Nature* **421,** 456–457 (2003).

39. Lukjancenko, O., Wassenaar, T. M. & Ussery, D. W. Comparison of 61 Sequenced Escherichia coli Genomes. *Microb. Ecol.* **60,** 708–720 (2010).

40. Lodinová-Zádníková, R. *et al.* The antibody response in breast-fed and non-breast-fed infants after artificial colonization of the intestine with Escherichia coli O83. *Pediatr. Res.* **29,** 396–399 (1991).

41. Cukrowska, B. *et al.* Specific proliferative and antibody responses of premature infants to intestinal colonization with nonpathogenic probiotic E. coli strain Nissle 1917. *Scand. J. Immunol.* **55,** 204–209 (2002).

42. Hilbert, D. W. in *E. coli Infect. Causes, Treat. Prev.* (Rogers, M. C. & Peterson, N. D.) 1–66 (Nova Science Publishers, Inc., 2011).

43. Marrie, T. J. *et al.* Community-acquired pneumonia due to Escherichia coli. *Clin. Microbiol. Infect.* **4,** 717–723 (1998).

44. Glauert, A. M. & Thornley, M. J. The topography of the bacterial cell wall. *Annu. Rev. Microbiol.* **23,** 159–198 (1969).

45. Bladen, H. A. & Mergenhagen, S. E. Ultrastructure of Veillonella and Morphological Correlation of an Outer Membrane with Particles Associated with Endotoxic Activity. *J. Bacteriol.* **88,** 1482–1492 (1964).

46. Kellenberger, E. & Ryter, A. Cell Wall and Cytoplasmic Membrane of Escherichia coli. *J. Biophys. Biochem.* **4,** 323–328 (1956).

47. Braun, V. & Wolff, H. The murein-lipoprotein linkage in the cell wall of Escherichia coli. *Eur. J. Biochem.* **14,** 387–391 (1970).

48. Park, J. S. *et al.* Mechanism of anchoring of OmpA protein to the cell wall peptidoglycan of the gram-negative bacterial outer membrane. *FASEB J.* **26,** 219–228 (2012).

49. Kamio, Y. & Nikaido, H. Outer membrane of Salmonella typhimurium: accessibility of phospholipid head groups to phospholipase c and cyanogen bromide activated dextran in the external medium. *Biochemistry* **15,** 2561–2570 (1976).

50. Leive, L. A Nonspecific Increase in Permeability in Escherichia Coli Produced By Edta. *Proc. Natl. Acad. Sci. U. S. A.* **53,** 745–750 (1965).

51. Hirota, Y., Suzuki, H., Nishimura, Y. & Yasuda, S. On the process of cellular division in Escherichia coli: a mutant of E. coli lacking a murein-lipoprotein. *Proc. Natl. Acad. Sci. U. S. A.* **74,** 1417–1420 (1977).

52. Locher, K. P. *et al.* Transmembrane signaling across the ligand-gated FhuA receptor: Crystal structures of free and ferrichrome-bound states reveal allosteric changes. *Cell* **95,** 771–778 (1998).

53. Chimento, D. P., Mohanty, A. K., Kadner, R. J. & Wiener, M. C. Substrate-induced transmembrane signaling in the cobalamin transporter BtuB. *Nat. Struct. Biol.* **10,** 394–401 (2003).

54. Pautsch, A. & Schulz, G. High-resolution structure of the OmpA membrane domain. *J. Mol. Biol.* **298,** 273–282 (2000).

55. Koebnik, R. Structural and functional roles of the surface-exposed loops of the beta-barrel membrane protein OmpA from Escherichia coli. *J. Bacteriol.* **181,** 3688–3694 (1999).

56. Danelon, C., Nestorovich, E. M., Winterhalter, M., Ceccarelli, M. & Bezrukov, S. M. Interaction of zwitterionic penicillins with the OmpF channel facilitates their translocation. *Biophys. J.* **90,** 1617–1627 (2006).

57. Im, W. & Roux, B. Ions and counterions in a biological channel: A molecular dynamics simulation of ompf porin from Escherichia coli in an explicit membrane with 1 M KCl aqueous salt solution. *J. Mol. Biol.* **319,** 1177–1197 (2002).

58. Alcaraz, A., Nestorovich, E. M., Aguilella-Arzo, M., Aguilella, V. M. & Bezrukov, S. M. Salting out the ionic selectivity of a wide channel: the asymmetry of OmpF. *Biophys. J.* **87,** 943–57 (2004).

59. Bredin, J. *et al.* Alteration of pore properties of Escherichia coli OmpF induced by mutation of key residues in anti-loop 3 region. *Biochem. J.* **363,** 521–528 (2002).

60. Phale, P. S. *et al.* Role of charged residues at the OmpF porin channel constriction probed by mutagenesis and simulation. *Biochemistry* **40,** 6319–6325 (2001).

61. Nestorovich, E. M., Rostovtseva, T. K. & Bezrukov, S. M. Residue ionization and ion transport through OmpF channels. *Biophys. J.* **85,** 3718–3729 (2003).

62. Dela Vega, A. L. & Delcour, A. H. Polyamines decrease Escherichia coli outer membrane permeability . These include : Polyamines Decrease Escherichia coli Outer Membrane Permeability. *J. Bacteriol.* **178,** 3715–3721 (1996).

63. Baslé, A., Iyer, R. & Delcour, A. H. Subconductance states in OmpF gating. *Biochim. Biophys. Acta - Biomembr.* **1664,** 100–107 (2004).

64. Iyer, R. & Delcour, A. H. Complex inhibition of OmpF and OmpC bacterial porins by polyamines. *J. Biol. Chem.* **272,** 18595–18601 (1997).

65. Benz, R., Schmid, A. & Hancock, R. E. W. Ion selectivity of gram-negative bacterial porins. *J. Bacteriol.* **162,** 722–727 (1985).

66. Cowan, S. W. *et al.* Crystal structures explain functional properties of two E. coli porins. *Nature* **358,** 727–733 (1992).

67. Bonhivers, M., Ghazi, A., Boulanger, P. & Letellier, L. FhuA, a transporter of the Escherichia coli outer membrane, is converted into a channel upon binding of bacteriophage T5. *EMBO J.* **15,** 1850–1856 (1996).

68. Saint, N., De, E., Julien, S., Orange, N. & Molle, G. Ionophore properties of OmpA of Escherichia coli. *Biochim. Biophys. Acta* **1145,** 119–123 (1993).

69. Vollmer, W., Blanot, D. & De Pedro, M. A. Peptidoglycan structure and architecture. *FEMS Microbiol. Rev.* **32,** 149–167 (2008).

70. Kühner, D., Stahl, M., Demircioglu, D. D. & Bertsche, U. From cells to muropeptide structures in 24 h: Peptidoglycan mapping by UPLC-MS. *Sci. Rep.* **4,** 7494 (2014).

71. Kralj, J., Hochbaum, D., Douglass, A. & Cohen, A. Electrical Spiking in Escherichia coli. *Science.* **333,** 345–348 (2011).

72. Hodgkin, A. L. & Huxley, A. F. A quantitative description of membrane current and its application to conduction and excitation in nerve. *J. Physiol.* **117,** 500–44 (1952).

73. Jiang, Y. *et al.* X-ray structure of a voltage-dependent K+ channel. *Nature* **423,** 33–41 (2003).

74. Long, S. B., Campbell, E. B. & Mackinnon, R. Crystal structure of a mammalian voltage-dependent Shaker family K+ channel. *Science.* **309,** 897–903 (2005).

75. Chen, X., Wang, Q., Ni, F. & Ma, J. Structure of the full-length Shaker potassium channel Kv1.2 by normal-mode-based X-ray crystallographic refinement. *Proc. Natl. Acad. Sci. U. S. A.* **107,** 11352–11357 (2010).

76.   MacKinnon, R., Cohen, S. L., Kuo, A., Lee, A. & Chait, B. T. Structural conservation in prokaryotic and eukaryotic potassium channels. *Science* **280,** 106–109 (1998).

77.   Doyle, D. A. *et al.* The structure of the potassium channel: molecular basis of K+ conduction and selectivity. *Science* **280,** 69–77 (1998).

78.   Hille, B. *Ion Channels of Excitable Membranes*. (Sinauer Associates, Inc., 2001).

79.   Strong, M., Chandy, K. G. & Gutman, G. A. Molecular evolution of voltage-sensitive ion channel genes: on the origins of electrical excitability. *Mol. Biol. Evol.* **10,** 221–242 (1993).

80.   Antz, C. & Fakler, B. Fast Inactivation of Voltage-Gated K(+) Channels: From Cartoon to Structure. *News Physiol. Sci.* **13,** 177–182 (1998).

81.   Zhou, Y. & MacKinnon, R. The occupancy of ions in the K+ selectivity filter: Charge balance and coupling of ion binding to a protein conformational change underlie high conduction rates. *J. Mol. Biol.* **333,** 965–975 (2003).

82.   Liu, S., Bian, X. & Lockless, S. W. Preferential binding of K+ ions in the selectivity filter at equilibrium explains high selectivity of K+ channels. *J. Gen. Physiol.* **140,** 671–679 (2012).

83.   Hille, B. & Schwarz, W. Potassium channels as multi-ion single-file pores. *J. Gen. Physiol.* **72,** 409–442 (1978).

84.   Hodgkin, A. L. & Keynes, R. D. The potassium permeability of a giant nerve fibre. *J. Physiol.* **128,** 61–88 (1955).

85.   Jensen, M. Ø. *et al.* Principles of conduction and hydrophobic gating in K+ channels. *Proc. Natl. Acad. Sci. U. S. A.* **107,** 5833–5838 (2010).

86.   Chong, H. L. & Ruben, P. C. Interaction between voltage-gated sodium channels and the neurotoxin, tetrodotoxin. *Channels* **2,** 407–412 (2008).

87.   Vitko, I. *et al.* The I-II loop controls plasma membrane expression and gating of Ca(v)3.2 T-type Ca2+ channels: a paradigm for childhood absence epilepsy mutations. *J. Neurosci.* **27,** 322–330 (2007).

88.   Steinlein, O. K. Ion channels and epilepsy. *Am. J. Med. Genet. - Semin. Med. Genet.* **106,** 146–159 (2001).

89.   Colombini, M. A candidate for the permeability pathway of the outer mitochondrial membrane. *Nature* **279,** 643–345 (1979).

90.	Schein, S. J., Colombini, M. & Finkelstein, A. Reconstitution in planar lipid bilayers of a voltage-dependent anion-selective channel obtained from paramecium mitochondria. *J. Membr. Biol.* **30,** 99–120 (1976).

91.	Mihara, K. & Sato, R. Molecular cloning and sequencing of cDNA for yeast porin, an outer mitochondrial membrane protein: a search for targeting signal in the primary structure. *EMBO J.* **4,** 769–74 (1985).

92.	Kleene, R. *et al.* Expression and Import Into Mitochondria. **6,** 2627–2633 (1987).

93.	Hodge, T. & Colombini, M. Regulation of metabolite flux through voltage-gating of VDAC channels. *J. Membr. Biol.* **157,** 271–279 (1997).

94.	Rostovtseva, T. & Colombini, M. ATP flux is controlled by a voltage-gated channel from the mitochondrial outer membrane. *J. Biol. Chem.* **271,** 28006–28008 (1996).

95.	Ludwig, O., De Pinto, V., Palmieri, F. & Benz, R. Pore formation by the mitochondrial porin of rat brain in lipid bilayer membranes. *Biochim. Biophys. Acta* **860,** 268–276 (1986).

96.	Song, J. & Colombini, M. Indications of a common folding pattern for VDAC channels from all sources. *J. Bioenerg. Biomembr.* **28,** 153–161 (1996).

97.	Mannella, C. A., Forte, M. & Colombini, M. Toward the molecular structure of the mitochondrial channel, VDAC. *J. Bioenerg. Biomembr.* **24,** 7–19 (1992).

98.	Colombini, M., Yeung, C. L., Tung, J. & König, T. The mitochondrial outer membrane channel, VDAC, is regulated by a synthetic polyanion. *Biochim. Biophys. Acta* **905,** 279–286 (1987).

99.	Ludwig, O., Krause, J., Hay, R. & Benz, R. Purification and characterization of the pore forming protein of yeast mitochondrial outer membrane. *Eur. Biophys. J.* **15,** 269–276 (1988).

100.	Song, J., Midson, C., Blachly-Dyson, E., Forte, M. & Colombini, M. The topology of VDAC as probed by biotin modification. *J. Biol. Chem.* **273,** 24406–24413 (1998).

101.	Blachly-Dyson, E., Peng, S., Colombini, M. & Forte, M. Selectivity changes in site-directed mutants of the VDAC ion channel: structural implications. *Science* **247,** 1233–1236 (1990).

102.	Hiller, S. *et al.* in Detergent Micelles. *Science* **321,** 1206–1210 (2008).

103. Ujwal, R. *et al.* The crystal structure of mouse VDAC1 at 2.3 A resolution reveals mechanistic insights into metabolite gating. *Proc. Natl. Acad. Sci. U. S. A.* **105,** 17742–17747 (2008).

104. Bayrhuber, M. *et al.* Structure of the human voltage-dependent anion channel. *Proc. Natl. Acad. Sci.* **105,** 15370–5 (2008).

105. Colombini, M. The published 3D structure of the VDAC channel: native or not? *Trends Biochem. Sci.* **34,** 382–9 (2009).

106. Saks, V. A. *et al.* Control of cellular respiration in vivo by mitochondrial outer membrane and by creatine kinase. A new speculative hypothesis: possible involvement of mitochondrial-cytoskeleton interactions. *J. Mol. Cell. Cardiol.* **27,** 625–645 (1995).

107. Maldonado, E. N. *et al.* Voltage-dependent anion channels modulate mitochondrial metabolism in cancer cells: Regulation by free tubulin and erastin. *J. Biol. Chem.* **288,** 11920–11929 (2013).

108. Rapizzi, E. *et al.* Recombinant expression of the voltage-dependent anion channel enhances the transfer of Ca2+ microdomains to mitochondria. *J. Cell Biol.* **159,** 613–624 (2002).

109. Shimizu, S., Narita, M. & Tsujimoto, Y. Bcl-2 family proteins regulate the release of apoptogenic cytochrome c by the mitochondrial channel VDAC. *Nature* **399,** 483–7 (1999).

110. Shoshan-Barmatz, V., Israelson, a., Brdiczka, D. & Sheu, S. The Voltage-Dependent Anion Channel (VDAC): Function in Intracellular Signalling, Cell Life and Cell Death. *Curr. Pharm. Des.* **12,** 2249–2270 (2006).

111. Yoo, B. C., Fountoulakis, M., Cairns, N. & Lubec, G. Changes of voltage-dependent anion-selective channel proteins VDAC1 and VDAC2 brain levels in patients with Alzheimer's disease and Down syndrome. *Electrophoresis* **22,** 172–179 (2001).

112. Shinohara, Y. *et al.* Characterization of porin isoforms expressed in tumor cells. *Eur. J. Biochem.* **267,** 6067–6073 (2000).

113. Zamarin, D., García-Sastre, A., Xiao, X., Wang, R. & Palese, P. Influenza virus PB1-F2 protein induces cell death through mitochondrial ANT3 and VDAC1. *PLoS Pathog.* **1,** 0040–0054 (2005).

114. Beyer, E. C. & Berthoud, V. M. in *Connexins A Guide.* (Harris, A. L. & Locke, D.) 3–26 (2009).

115. Oh, S., Verselis, V. K. & Bargiello, T. A. Charges dispersed over the permeation pathway determine the charge selectivity and conductance of a Cx32 chimeric hemichannel. *J. Physiol.* **586,** 2445–2461 (2008).

116. Oh, S. *et al.* Changes in permeability caused by connexin 32 mutations underlie X- linked Charcot-Marie-Tooth disease. *Neuron* **19,** 927–938 (1997).

117. Barrio, L. C. *et al.* Gap junctions formed by connexins 26 and 32 alone and in combination are differently affected by applied voltage. *Proc. Natl. Acad. Sci. U. S. A.* **88,** 8410–8414 (1991).

118. Bargiello, T. A., Tang, Q., Oh, S. & Kwon, T. Voltage-dependent conformational changes in connexin channels. *Biochim. Biophys. Acta* **29,** 997–1003 (2012).

119. Verselis, V. K., Ginter, C. S. & Bargiello, T. A. Opposite voltage gating polarities of two closely related connexins. *Nature* **368,** 348–351 (1994).

120. Oh, S., Rivkin, S., Tang, Q., Verselis, V. K. & Bargiello, T. A. Determinants of gating polarity of a connexin 32 hemichannel. *Biophys. J.* **87,** 912–928 (2004).

121. Shibayama, J. *et al.* Effect of charge substitutions at residue his-142 on voltage gating of connexin43 channels. *Biophys. J.* **91,** 4054–4063 (2006).

122. Moreno, A. P. *et al.* Role of the carboxyl terminal of connexin43 in transjunctional fast voltage gating. *Circ. Res.* **90,** 450–457 (2002).

123. Anumonwo, J. M. *et al.* The carboxyl terminal domain regulates the unitary conductance and voltage dependence of connexin40 gap junction channels. *Circ. Res.* **88,** 666–673 (2001).

124. Oh, S. & Bargiello, T. A. Voltage Regulation of Connexin Channel Conductance. *Yonsei Med. J.* **56,** 1–15 (2015).

125. Thimm, J., Mechler, A., Lin, H., Rhee, S. & Lal, R. Calcium-dependent open/closed conformations and interfacial energy maps of reconstituted hemichannels. *J. Biol. Chem.* **280,** 10646–10654 (2005).

126. Pfenniger, A., Wohlwend, A. & Kwak, B. R. Mutations in connexin genes and disease. *Eur. J. Clin. Invest.* **41,** 103–116 (2011).

127. Abrams, C. K. *et al.* Functional requirement for a highly conserved charged residue at position 75 in the gap junction protein connexin 32. *J. Biol. Chem.* **288,** 3609–3619 (2013).

128. Dong, C. *et al.* Wza the translocon for E. coli capsular polysaccharides defines a new class of membrane protein. *Nature* **444,** 226–229 (2006).

129. Schindler, H. & Rosenbusch, J. P. Matrix protein from Escherichia coli outer membranes forms voltage-controlled channels in lipid bilayers. *Proc. Natl. Acad. Sci. U. S. A.* **75,** 3751–5 (1978).

130. Characterization, I. I. F. *et al.* Structural and Functional Characterization of OmpF Porin Mutants Selected for Larger Pore Size. *J. Biol. Chem.* **271,** 20676–20680 (1996).

131. Rudel, T. *et al.* Modulation of Neisseria porin (PorB) by cytosolic ATP/GTP of target cells: Parallels between pathogen accommodation and mitochondrial endosymbiosis. *Cell* **85,** 391–402 (1996).

132. Sen, K., Hellman, J. & Nikaido, H. Porin channels in intact cells of Escherichia coli are not affected by Donnan potentials across the outer membrane. *J. Biol. Chem.* **263,** 1182–1187 (1988).

133. Eppens, E. F., Saint, N., Van Gelder, P., Van Boxtel, R. & Tommassen, J. Role of the constriction loop in the gating of outer membrane porin PhoE of Escherichia coli. *FEBS Lett.* **415,** 317–320 (1997).

134. Todt, J. C., Rocque, W. J. & McGroarty, E. J. Effects of pH on bacterial porin function. *Biochemistry* **31,** 10471–10478 (1992).

135. Wiese, A. *et al.* Influence of the lipid matrix on incorporation and function of LPS-free porin from Paracoccus denitrificans. *Biochim. Biophys. Acta* **1190,** 231–242 (1994).

136. Hagge, S. O. *et al.* Pore formation and function of phosphoporin phoE of Escherichia coli are determined by the core sugar moiety of lipopolysaccharide. *J. Biol. Chem.* **277,** 34247–34253 (2002).

137. Iyer, R., Wu, Z., Woster, P. M. & Delcour, A. H. Molecular basis for the polyamine-ompF porin interactions: inhibitor and mutant studies. *J. Mol. Biol.* **297,** 933–945 (2000).

138. Samartzidou, H. & Delcour, A. H. Distinct sensitivities of OmpF and PhoE porins to charged modulators. *FEBS Lett.* **444,** 65–70 (1999).

139. Lakey, J. H. & Pattus, F. The voltage-dependent activity of Escherichia coli porins in different planar bilayer reconstitutions. *Eur. J. Biochem.* **186,** 303–308 (1989).

140. Karshikoff, A., Spassov, V., Cowan, S. W., Ladenstein, R. & Schirmer, T. Electrostatic properties of two porin channels from Escherichia coli. *J. Mol. Biol.* **240,** 372–384 (1994).

141. Tieleman, D. P. & Berendsen, H. J. A molecular dynamics study of the pores formed by Escherichia coli OmpF porin in a fully hydrated palmitoyloleoylphosphatidylcholine bilayer. *Biophys. J.* **74,** 2786–2801 (1998).

142. Phale, P. S. *et al.* Voltage gating of Escherichia coli porin channels: role of the constriction loop. *Proc. Natl. Acad. Sci. U. S. A.* **94,** 6741–6745 (1997).

143. Bainbridge, G., Mobasheri, H., Armstrong, G. A, Lea, E. J. & Lakey, J. H. Voltage-gating of Escherichia coli porin: a cystine-scanning mutagenesis study of loop 3. *J. Mol. Biol.* **275,** 171–176 (1998).

144. Hirano-Iwata, A. *et al.* Free-Standing Lipid Bilayers in Silicon Chips-Membrane Stabilization Based on Microfabricated Apertures with a Nanometer-Scale Smoothness. *Langmuir* 22–25 (2009).

145. Arbing, M. A., Hanrahan, J. W. & Coulton, J. W. Mutagenesis identifies amino acid residues in extracellular loops and within the barrel lumen that determine voltage gating of porin from Haemophilus influenzae type b. *Biochemistry* **40,** 14621–14628 (2001).

146. Arbing, M. A. *et al.* Charged residues in surface-located loops influence voltage gating of porin from haemophilus influenzae type b. *J. Membr. Biol.* **178,** 185–193 (2000).

147. Kang, J., Huguenard, J. R. & Prince, D. A. Voltage-gated potassium channels activated during action potentials in layer V neocortical pyramidal neurons. *J. Neurophysiol.* **83,** 70–80 (2000).

148. Jiang, Y. *et al.* The open pore conformation of potassium channels. *Nature* **417,** 523–526 (2002).

149. Seoh, S. A, Sigg, D., Papazian, D. M. & Bezanilla, F. Voltage-sensing residues in the S2 and S4 segments of the Shaker K+ channel. *Neuron* **16,** 1159–67 (1996).

150. Starace, D. M. & Bezanilla, F. Histidine scanning mutagenesis of basic residues of the S4 segment of the shaker k+ channel. *J. Gen. Physiol.* **117,** 469–490 (2001).

151. Schoppa, N. E., McCormack, K., Tanouye, M. A. & Sigworth, F. J. The size of gating charge in wild-type and mutant Shaker potassium channels. *Science* **255,** 1712–5 (1992).

152. Schmidt, D. & MacKinnon, R. Voltage-dependent K+ channel gating and voltage sensor toxin sensitivity depend on the mechanical state of the lipid membrane. *Proc. Natl. Acad. Sci. U. S. A.* **105,** 19276–19281 (2008).

153. Colombini, M. Voltage gating in the mitochondrial channel, VDAC. *J. Membr. Biol.* **111,** 103–11 (1989).

154. Doring, C. & Colombini, M. Voltage dependence and ion selectivity of the mitochondrial channel, VDAC, are modified by succinic anhydride. *J. Membr. Biol.* **83,** 81–86 (1985).

155. Roos, N., Benz, R. & Brdiczka, D. Identification and characterization of the pore-forming protein in the outer membrane of rat liver mitochondria. *Biochim. Biophys. Acta* **686,** 204–214 (1982).

156. Zizi, M., Byrd, C., Boxus, R. & Colombini, M. The voltage-gating process of the voltage-dependent anion channel is sensitive to ion flow. *Biophys. J.* **75,** 704–713 (1998).

157. Van Gelder, P. *et al.* Voltage sensing in the PhoE and OmpF outer membrane porins of Escherichia coli: role of charged residues. *J. Mol. Biol.* **269,** 468–472 (1997).

158. Benz, R. *Bacterial and Eukaryotic Porins*. (Wiley-VCH, 2004).

159. Montal, M. & Mueller, P. Formation of bimolecular membranes from lipid monolayers and a study of their electrical properties. *Proc. Natl. Acad. Sci. U. S. A.* **69,** 3561–6 (1972).

160. Colombini, M. Characterization of Channels Isolated from Plant Mitochondria. *Methods Enzymol.* **148,** 465 (1987).

161. Hodgkin, A. & Katz, B. The Effect Of Sodium Ions On The Electrical Activity Of The Giant Axon Of The Squid. *J. Physiol.* **108,** 37–77 (1949).

162. Goldman, D. E. Potential, Impedance, And Rectification In Membranes. *J. Gen. Physiol.* **27,** 37–60 (1943).

163. Hall, J. E. Access resistance of a small circular pore. *J. Gen. Physiol.* **66,** 531–2 (1975).

164. Suzuki, M., Youle, R. J. & Tjandra, N. Structure of Bax: coregulation of dimer formation and intracellular localization. *Cell* **103,** 645–54 (2000).

165. Youle, R. J. & Strasser, A. The BCL-2 protein family: opposing activities that mediate cell death. *Nat. Rev. Mol. Cell Biol.* **9,** 47–59 (2008).

166. Kuwana, T. *et al.* Bid, Bax, and lipids cooperate to form supramolecular openings in the outer mitochondrial membrane. *Cell* **111,** 331–42 (2002).

167. Letai, A. *et al.* Distinct BH3 domains either sensitize or activate mitochondrial apoptosis, serving as prototype cancer therapeutics. *Cancer Cell* **2,** 183–92 (2002).

168. Kim, H. *et al.* Hierarchical regulation of mitochondrion-dependent apoptosis by BCL-2 subfamilies. *Nat. Cell Biol.* **8,** 1348–58 (2006).

169. Willis, S. N. *et al.* Apoptosis initiated when BH3 ligands engage multiple Bcl-2 homologs, not Bax or Bak. *Science* **315,** 856–9 (2007).

170. Chen, L. *et al.* Differential targeting of prosurvival Bcl-2 proteins by their BH3-only ligands allows complementary apoptotic function. *Mol. Cell* **17,** 393–403 (2005).

171. Lalier, L. *et al.* Bax activation and mitochondrial insertion during apoptosis. *Apoptosis* **12,** 887–96 (2007).

172. Gavathiotis, E., Reyna, D. E., Davis, M. L., Bird, G. H. & Walensky, L. D. BH3-triggered structural reorganization drives the activation of proapoptotic BAX. *Mol. Cell* **40,** 481–92 (2010).

173. Gavathiotis, E. *et al.* BAX activation is initiated at a novel interaction site. *Nature* **455,** 1076–81 (2008).

174. Bleicken, S. *et al.* Molecular details of Bax activation, oligomerization, and membrane insertion. *J. Biol. Chem.* **285,** 6636–47 (2010).

175. Zhang, Z. *et al.* Bax forms an oligomer via separate, yet interdependent, surfaces. *J. Biol. Chem.* **285,** 17614–27 (2010).

176. George, N. M., Evans, J. J. D. & Luo, X. A three-helix homo-oligomerization domain containing BH3 and BH1 is responsible for the apoptotic activity of Bax. *Genes Dev.* **21,** 1937–48 (2007).

177. Westphal, D., Dewson, G., Czabotar, P. E. & Kluck, R. M. Molecular biology of Bax and Bak activation and action. *Biochim. Biophys. Acta* **1813,** 521–531 (2010).

178. Leber, B., Lin, J. & Andrews, D. W. Still embedded together binding to membranes regulates Bcl-2 protein interactions. *Oncogene* **29,** 5221–30 (2010).

179. Antonsson, B. *et al.* Inhibition of Bax Channel-Forming Activity by Bcl-2. *Science* **277,** 370–372 (1997).

180. Schlesinger, P. H. *et al.* Comparison of the ion channel characteristics of proapoptotic BAX and antiapoptotic BCL-2. *Proc. Natl. Acad. Sci. U. S. A.* **94,** 11357–62 (1997).

181. Schlesinger, P. H. & Saito, M. The Bax pore in liposomes, Biophysics. *Cell Death Differ.* **13,** 1403–8 (2006).

182. Basañez, G. *et al.* Bax, but not Bcl-xL, decreases the lifetime of planar phospholipid bilayer membranes at subnanomolar concentrations. *Proc. Natl. Acad. Sci. U. S. A.* **96,** 5492–7 (1999).

183. Jonas, E. A., Hardwick, J. M. & Kaczmarek, L. K. Actions of BAX on Mitochondrial Channel Activity and on Synaptic Transmission. *Antioxid. Redox Signal.* **7,** 1092–1100 (2005).

184. Martinez-Caballero, S. *et al.* Assembly of the mitochondrial apoptosis-induced channel, MAC. *J. Biol. Chem.* **284,** 12235–45 (2009).

185. Kagawa, Y. & Racker, E. Partial Resolution of the Enzymes Catalyzing Oxidative. *J. Biol. Chem.* **246,** 5477–5487 (1971).

186. Brustovetsky, T. *et al.* BAX insertion, oligomerization, and outer membrane permeabilization in brain mitochondria: role of permeability transition and SH-redox regulation. *Biochim. Biophys. Acta* **1797,** 1795–806 (2010).

187. Goldman, D. E. Potential, Impedance, and Rectification in Membranes. *J. Gen. Physiol.* **27,** 37–60 (1943).

188. Xu, X. & Colombini, M. Self-catalyzed insertion of proteins into phospholipid membranes. *J. Biol. Chem.* **271,** 23675–82 (1996).

189. Petersheim, M. & Sun, J. On the coordination of La3+ by phosphatidylserine. *Biophys. J.* **55,** 631–6 (1989).

190. Brown, M. & Seelig, J. Ion-induced changes in head group conformation of lecithin bilayers. *Nature* **269,** 721–723 (1977).

191. Seelig, J., Macdonald, P. M. & Scherer, P. G. Phospholipid Head Groups as Sensors of Electric Charge in Membranes. *Biochemistry* **26,** 7535–7541 (1987).

192. Tanaka, T., Tamba, Y., Masum, S. M., Yamashita, Y. & Yamazaki, M. La(3+) and Gd(3+) induce shape change of giant unilamellar vesicles of phosphatidylcholine. *Biochim. Biophys. Acta* **1564,** 173–82 (2002).

193. Ermakov, Y. A., Kamaraju, K., Sengupta, K. & Sukharev, S. Gadolinium ions block mechanosensitive channels by altering the packing and lateral pressure of anionic lipids. *Biophys. J.* **98,** 1018–27 (2010).

194. Pavlov, E. V *et al.* A novel, high conductance channel of mitochondria linked to apoptosis in mammalian cells and Bax expression in yeast. *J. Cell Biol.* **155,** 725–31 (2001).

195. Annis, M. G. *et al.* Bax forms multispanning monomers that oligomerize to permeabilize membranes during apoptosis. *EMBO J.* **24,** 2096–103 (2005).

196. García-Sáez, A. J., Mingarro, I., Pérez-Payá, E. & Salgado, J. Membrane-insertion fragments of Bcl-xL, Bax, and Bid. *Biochemistry* **43,** 10930–43 (2004).

197. Saito, M., Korsmeyer, S. J., Schlesinger, P. H., Farber, D. & Hughes, H. Bax-dependent transport of cytochrome c reconstituted in pure liposomes. *Nat. Cell Biol.* **2,** 553–555 (2000).

198. Nechushtan, A., Smith, C. L., Lamensdorf, I., Yoon, S. H. & Youle, R. J. Bax and Bak coalesce into novel mitochondria-associated clusters during apoptosis. *J. Cell Biol.* **153,** 1265–76 (2001).

199. Ross, K., Rudel, T. & Kozjak-Pavlovic, V. TOM-independent complex formation of Bax and Bak in mammalian mitochondria during TNFalpha-induced apoptosis. *Cell Death Differ.* **16,** 697–707 (2009).

200. Colombini, M. VDAC: the channel at the interface between mitochondria and the cytosol. *Mol. Cell. Biochem.* **256-257,** 107–15 (2004).

201. Lemeshko, V. V. Model of the outer membrane potential generation by the inner membrane of mitochondria. *Biophys. J.* **82,** 684–92 (2002).

202. Porcelli, A. M. *et al.* pH difference across the outer mitochondrial membrane measured with a green fluorescent protein mutant. *Biochem. Biophys. Res. Commun.* **326,** 799–804 (2005).

203. Ausili, A., Torrecillas, A., Martínez-Senac, M. M., Corbalán-García, S. & Gómez-Fernández, J. C. The interaction of the Bax C-terminal domain with negatively charged lipids modifies the secondary structure and changes its way of insertion into membranes. *J. Struct. Biol.* **164,** 146–52 (2008).

204. Kizer, N., Harter, L., Hruska, K., Alvarez, U. & Duncan, R. Volume regulatory decrease in UMR-106.01 cells is mediated by specific alpha1 subunits of L-type calcium channels. *Cell Biochem. Biophys.* **31,** 65–79 (1999).

205. Best, L., Brown, P. D., Sener, A. & Malaisse, W. J. Electrical activity in pancreatic islet cells: The VRAC hypothesis. *Islets* **2,** 59–64 (2010).

206. DeCoursey, T. E. Voltage-gated proton channels: molecular biology, physiology, and pathophysiology of the H(V) family. *Physiol. Rev.* **93,** 599–652 (2013).

207. Bainbridge, G., Gokce, I. & Lakey, J. H. Voltage gating is a fundamental feature of porin and toxin beta-barrel membrane channels. *FEBS Lett.* **431,** 305–8 (1998).

208. Colombini, M. Mitochondrial Outer Membrane Channels. *Chem. Rev.* **112,** 6373–6387 (2012).

209. Lin, S. H. *et al.* Bax forms two types of channels, one of which is voltage-gated. *Biophys. J.* **101,** 2163–9 (2011).

210. Rostovtseva, T. K. *et al.* Bid, but not Bax, regulates VDAC channels. *J. Biol. Chem.* **279,** 13575–83 (2004).

211. Miller, C. & White, M. M. Dimeric structure of single chloride channels from Torpedo electroplax. *Proc. Natl. Acad. Sci.* **81,** 2772–2775 (1984).

212. Weiss, M. S., Wacker, T., Weckesser, J., Welte, W. & Schulz, G. E. The three-dimensional structure of porin from Rhodobacter capsulatus at 3 A resolution. *FEBS Lett.* **267,** 268–72 (1990).

213. Hsu, Y. T. & Youle, R. J. Nonionic detergents induce dimerization among members of the Bcl-2 family. *J. Biol. Chem.* **272,** 13829–34 (1997).

214. Gross, A., Jockel, J., Wei, M. C. & Korsmeyer, S. J. Enforced dimerization of BAX results in its translocation, mitochondrial dysfunction and apoptosis. *EMBO J.* **17,** 3878–85 (1998).

215. Eskes, R., Desagher, S., Antonsson, B. & Martinou, J. C. Bid induces the oligomerization and insertion of Bax into the outer mitochondrial membrane. *Mol. Cell. Biol.* **20,** 929–35 (2000).

216. Henrickson, S. E., DiMarzio, E. A., Wang, Q., Stanford, V. M. & Kasianowicz, J. J. Probing single nanometer-scale pores with polymeric molecular rulers. *J. Chem. Phys.* **132,** 135101–135108 (2010).

217. Zizi, M., Thomas, L., Blachly-Dyson, E., Forte, M. & Colombini, M. Oriented Channel Insertion Reveals the Motion of a Transmembrane Beta Strand During Voltage Gating of VDAC. *J. Membr. Biol.* **144,** 121–129 (1995).

218. Kienker, P. K., Jakes, K. S. & Finkelstein, A. Protein translocation across planar bilayers by the colicin Ia channel-forming domain: where will it end? *J. Gen. Physiol.* **116,** 587–98 (2000).

219. Schoppa, N. E., McCormack, K., Tanouye, M. A. & Sigworth, F. J. The size of gating charge in wild-type and mutant Shaker potassium channels. *Science* **255,** 1712–5 (1992).

220. Aggarwal, S. K. & MacKinnon, R. Contribution of the S4 segment to gating charge in the Shaker K+ channel. *Neuron* **16,** 1169–77 (1996).

221. Dewson, G. *et al.* Bax dimerizes via a symmetric BH3:groove interface during apoptosis. *Cell Death Differ.* **19,** 661–70 (2012).

222. Czabotar, P. E. *et al.* Bax crystal structures reveal how BH3 domains activate Bax and nucleate its oligomerization to induce apoptosis. *Cell* **152,** 519–31 (2013).

223. Noda, M. *et al.* Primary structure of Electrophorus electricus sodium channel deduced from cDNA sequence. *Nature* **312,** 121–7 (1984).

224. Colombini, M. VDAC structure, selectivity, and dynamics. *Biochim. Biophys. Acta* **1818,** 1457–65 (2012).

225. Thomas, L., Blachly-Dyson, E., Colombini, M. & Forte, M. Mapping of residues forming the voltage sensor of the voltage-dependent anion-selective channel. *Proc. Natl. Acad. Sci. U. S. A.* **90,** 5446–9 (1993).

226. Nikaido, H. Preventing drug access to targets: cell surface permeability barriers and active efflux in bacteria. *Semin. Cell Dev. Biol.* **12,** 215–223 (2001).

227. Nikaido, H. Molecular basis of bacterial outer membrane permeability revisited. *Microbiol. Mol. Biol. Rev.* **67,** 593–656 (2003).

228. Tran, Q. H. & Unden, G. Changes in the proton potential and the cellular energetics of Escherichia coli during growth by aerobic and anaerobic respiration or by fermentation. *Eur. J. Biochem.* **251,** 538–543 (1998).

229. Nikaido, H. Prevention of drug access to bacterial targets: permeability barriers and active efflux. *Science* **264,** 382–388 (1994).

230. Nikaido, H. & Normark, S. Sensitivity of Escherichia coli to various beta-lactams is determined by the interplay of outer membrane permeability and degradation by periplasmic beta-lactamases: a quantitative predictive treatment. *Mol. Microbiol.* **1,** 29–36 (1987).

231. Hocquet, D., Bertrand, X., Köhler, T., Talon, D. & Plésiat, P. Genetic and phenotypic variations of a resistant Pseudomonas aeruginosa epidemic clone. *Antimicrob. Agents Chemother.* **47,** 1887–1894 (2003).

232. Medeiros, A. A., O'Brien, T. F., Rosenberg, E. Y. & Nikaido, H. Loss of OmpC porin in a strain of Salmonella typhimurium causes increased resistance to cephalosporins during therapy. *J. Infect. Dis.* **156,** 751–757 (1987).

233. Chevalier, J., Pagès, J. M. & Malléa, M. In vivo modification of porin activity conferring antibiotic resistance to Enterobacter aerogenes. *Biochem. Biophys. Res. Commun.* **266,** 248–251 (1999).

234. Dé, E. *et al.* A new mechanism of antibiotic resistance in Enterobacteriaceae induced by a structural modification of the major porin. *Mol. Microbiol.* **41,** 189–198 (2001).

235. Deng, X. *et al.* Expression of multidrug resistance efflux pump gene norA Is iron responsive in Staphylococcus aureus. *J. Bacteriol.* **194,** 1753–1762 (2012).

236. Pumbwe, L. & Piddock, L. J. V. Two efflux systems expressed simultaneously in multidrug-resistant Pseudomonas aeruginosa. *Antimicrob. Agents Chemother.* **44,** 2861–2864 (2000).

237. Mohammad, M. M., Howard, K. R. & Movileanu, L. Redesign of a plugged beta-barrel membrane protein. *J. Biol. Chem.* **286,** 8000–13 (2011).

238. Mohammad, M. M., Howard, K. R. & Movileanu, L. Redesign of a plugged beta-barrel membrane protein. *J. Biol. Chem.* **286,** 8000–8013 (2011).

239. Lakey, J. H., Lea, E. J. & Pattus, F. ompC mutants which allow growth on maltodextrins show increased channel size and greater voltage sensitivity. *FEBS Lett.* **278,** 31–34 (1991).

240. Saint, N. *et al.* Replacement of the sole histidinyl residue in OmpF porin from E. coli by threonine (H21T) does not affect channel structure and function. *Biochem. Biophys. Res. Commun.* **223,** 118–122 (1996).